SERI/STR-211-2765
(DE85016881)

Energy

SOLAR

AMORPHOUS SILICON PHOTOVOLTAIC DEVICES PREPARED BY CHEMICAL AND PHOTOCHEMICAL VAPOR DEPOSITION OF HIGHER ORDER SILANES

Annual Subcontract Progress Report for the Period September 1, 1984—August 31, 1985

By
A. E. Delahoy
F. B. Ellis, Jr.

November 1985

Work Performed Under Contract No. AC02-83CH10093

Chronar Corporation
Princeton, New Jersey

and

Solar Energy Research Institute
Golden, Colorado

Technical Information Center
Office of Scientific and Technical Information
United States Department of Energy

DISCLAIMER

Available from the National Technical Information Service, U. S. Department of Commerce, Springfield, Virginia 22161.

Price: Printed Copy A03
Microfiche A01

Codes are used for pricing all publications. The code is determined by the number of pages in the publication. Information pertaining to the pricing codes can be found in the current issues of the following publications, which are generally available in most libraries: *Energy Research Abstracts (ERA); Government Reports Announcements* and Index *(GRA* and I); *Scientific and Technical Abstract Reports (STAR);* and publication NTIS-PR-360 available from NTIS at the above address.

Printed in the United States of America
USDOE Office of Scientific and Technical Information
Oak Ridge, Tennessee

SERI/STR-211-2765
(DE85016881)
Distribution Category UC-63

Amorphous Silicon Photovoltaic Devices Prepared by Chemical and Photochemical Vapor Deposition of Higher Order Silanes

Annual Subcontract Progress Report
1 September 1984 - 31 August 1985

A. E. Delahoy
F. B. Ellis, Jr.

Chronar Corporation
Princeton, New Jersey

November 1985

Prepared under Subcontract No. XB-5-04092-1
SERI Technical Monitor: B. Stafford

Solar Energy Research Institute
A Division of Midwest Research Institute

1617 Cole Boulevard
Golden, Colorado 80401

Prepared for the
U.S. Department of Energy
Contract No. DE-AC02-83CH10093

PREFACE

This report describes the preparation of hydrogenated amorphous silicon (a-Si:H) films and photovoltaic devices by chemical vapor deposition (CVD) from higher order silanes, and the properties of such films and devices. The research is directed at exploring new deposition techniques that ultimately could produce a-Si:H superior in some ways to that achieved by the well-known glow-discharge method. For example, improvements could stem from ease of deposition (lower cost and/or better reproducibility), from material improvement (higher efficiency and/or better stability under illumination), or from new innovative materials that improve device performance. In accordance with this objective, our research efforts have focussed on photo-CVD techniques and thermal CVD has been deemphasized. However, this report briefly discusses our reasons for terminating our research of thermal CVD films. The bulk of this report presents results on deposition by mercury sensitized decomposition of disilane. These results indicate that this technique is a very promising alternative to the glow-discharge method.

The research was perfomed by A.E. Delahoy, Principal Investigator/Program Manager, F.B. Ellis, Jr., M. Akhtar, T. Tonon, J. Van Dine, and B. Doele.

We are indebted to Mr. A. Lichter for the in-house preparation of higher silanes of exceptional purity. Thanks are also due to Dr. W.E. Carlos (Naval Research Laboratory) for ESR measurements, Dr. W.A. Lanford (SUNY) for the nuclear reaction analysis, Dr. B. Wilson (AT and T Bell Labs) for photoluminescence experiments, Dr. B.G. Bagley (Bell Communications Research) for infra-red measurements, Dr. T. Horning for surface photovoltage measurements, Mr. J. Dick (SERI) for early SIMS analyses, and Mr. F. Ramos for Auger and SIMS analyses.

SUMMARY

Research performed under subcontract No. XB-5-04092-1 (Amorphous Silicon Photovoltaic Devices Prepared by Chemical and Photochemical Vapor Deposition of Higher Order Silanes) for the twelve-month period 9/1/84 - 8/31/85 is described. The work is summarized here.

Objectives

The program objectives are to continue characterization and development of a-Si:H by promising CVD techniques using higher order silanes. Reactor design and deposition conditions will be varied to optimize growth rate and properties of doped and undoped layers. The quality of the films will be evaluated from material composition, optoelectronic properties, and device performance. Specific goals include deposition of films at least 0.5 μm in thickness by photo-CVD, the attainment of an external current density of 10 mA/cm^2, and a single-junction efficiency of 6%. These objectives have been met--films about 2 μm in thickness can be deposited, external current densities greater than 13 mA/cm^2 are obtained, and a single junction efficiency of 6% has been produced.

Discussion

Different deposition techniques have been extensively explored in earlier contracts, including static CVD (principally 1982-1983), flow CVD (principally 1983-1984), and photo-CVD (principally 1983-present). Flow thermal CVD, compared to static thermal CVD, was shown to produce superior material for photovoltaic devices. We believe that the main advantage arises from its ability to deposit from optimal time-invariant gas-phase chemistry. Different optimization studies and the development of new layers, including a low-temperature, wide-band-gap p-layer, yielded device efficiencies of only 3-3.5% and fill factors that never exceeded 0.56. The main problem with thermal CVD is the poor quality of the i-layer--inferior photoconductivity in undoped films and unpaired electron spin densities of about 10^{17} spins per cm^3. We believe that the main reasons for the inferior i-layer in thermal CVD stems from the necessarily higher deposition temperature (above 400°C for an appreciable deposition rate). During the deposition of a-Si:H, because of the high deposition temperature, some hydrogen which normally would cap dangling bonds may be driven from the material. The loss of this hydrogen may create additional neutral defects. Thus, even though the CVD films have been measured to have about 17 atomic percent hydrogen using the nuclear reaction technique, if only a fraction of this hydrogen were lost during deposition (say 0.1 percent) it could produce the high defect density observed for CVD material. If this is the case, it imposes a fundamental limitation on the quality of thermal CVD material. Also, because of the high deposition temperature, there is a greater possibility of contamination by diffusion across the substrate-film interface.

For these reasons research in this contract has focussed on mercury sensitized decomposition of disilane where deposition temperatures are typically 200-250°C. Until recently, films prepared by this technique had a growth rate of about 0.2-0.3 A/s and were limited to about 0.3 μm in thickness because deposition on the Suprasil quartz window reduced the light intensity within the deposition chamber. The above growth rate and thickness were made possible by coating the window with a low-vapor-pressure

fluorocarbon oil (a perfluoropolyether) [1]. To better understand and overcome this problem, a laser thickness monitor was installed and static rate of pressure rise experiments were developed. We are pleased to report that through the use of a new reactor design and the above coating, deposition rates of up to 3 A/s and films about 2 μm in thickness have been obtained.

Research is under way to determine whether a diffusion barrier between the tin oxide and the a-Si:H, which appeared necessary for thermal CVD devices, would still be beneficial for photo-CVD (or glow-discharge) deposition.

Undoped a-Si:H films prepared by photo-CVD have a band gap which extends from under 1.76 to over 1.88 eV depending largely on the substrate temperature. The i-layer band gap for device use is generally 1.78-1.80 eV. These latter films have an AM1 photoconductivity between $1x10^{-5}$ and $2x10^{-3}$ $(\Omega\ cm)^{-1}$. The temperature dependence of the photoconductivity of these i-layers exhibits a low temperature peak and thermal quenching between 125 and 200 K.

A new, wide-band-gap p-layer was developed. This p-layer is deposited from mixtures of disilane, dimethylsilane, and diborane. Using equal mixtures of disilane and dimethylsilane and a diborane-to-total-silane ratio of 0.3% yielded a p-layer with a dark conductivity of $7x10^{-6}$ $(\Omega\text{-cm})^{-1}$ and an optical band gap of 1.97 eV. Omission of the dimethylsilane gives a p-layer with a gap of 1.66 eV.

Devices made using the wide band gap p-layer and the low (0.2-0.3 A/s) deposition rate i-layer already meet or exceed the device milestone specifications. Best device efficiency is 6.0%. Best individual device parameters are an open-circuit voltage (V_{oc}) greater than 0.81 V (if one includes devices with a fill factor less than 40% then V_{oc}'s > 0.9 V have been obtained), a fill factor (ff) greater than 0.66, and a short-circuit density (J_{sc}) greater than 13 mA/cm^2. A SIMS depth profile of a p-i-n device deposited by photo-CVD reveals a sharp p/i interface and suggests a boron shoulder about 0.05 μm wide. Dissociation of the tin oxide is not apparent.

The first 2-μm-thick film deposited at 2.2 A/s had a respectable diffusion length of 0.27 μm as measured by our new surface photovoltage setup. ESR measurements on other films deposited at a high growth rate indicate a low spin density ($1x10^{16}$ spins/cm^3).

Films deposited by mercury-sensitized photo-CVD exhibit the well-known Staebler-Wronski effect, i.e., photoconductivity of i-layers decreases under illumination, and photo-CVD devices degrade under AM1 light soaking and laser light soaking. The degradation is about a factor of two less than what is often seen in devices prepared by glow discharge. However, the photo-CVD devices had thinner i-layers which are known to reduce light-induced degradation. Therefore, we cannot yet report on whether it may be easier to reduce light-induced degradation by using photo-CVD. Original device performance can be almost completely restored by annealing at temperatures as low as 85°C.

Conclusions

A good i-layer is critical to high-efficiency devices. Unlike those for thermal CVD, our photo-CVD device results demonstrate that this method is capable of depositing quality i-layers, albeit at low deposition rates. The respectable diffusion length and low spin density obtained before optimization under conditions giving the higher growth rates (1-3 A/s) suggest that high-efficiency devices are possible for devices deposited in this growth-rate range. The higher growth rate is important for large-scale production. Consequently, material and device optimization at higher growth rates constitute a large part of the current research efforts. Other research is concerned with novel materials (e.g., wide-band-gap layers and microcrystalline layers) and novel device structures (e.g., graded i- or p-layers). A new system is also being built for deposition over a larger area and to further increase the deposition rate.

TABLE OF CONTENTS

LIST OF FIGURES

LIST OF TABLES

ABSTRACT

This report describes the preparation of hydrogenated amorphous silicon (a-Si:H) films and photovoltaic devices by chemical vapor deposition (CVD) from higher order silanes and the properties of such films and devices. The research explored new deposition techniques that could produce a-Si:H superior to that achieved by the glow-discharge method. For example, the improvement could stem from ease of deposition (lower cost and/or better reproducibility), from material improvement (higher efficiency and/or better stability under illumination), or from innovative materials that improve device performance. Research focused on photo-CVD techniques; thermal CVD was deemphasized. This report presents results for deposition by mercury-sensitized decomposition of disilane. These results indicate that this technique is a very promising alternative to the glow-discharge method.

SECTION 1
INTRODUCTION

1.1 PREPARATION OF HIGHER SILANES

Under our previous contracts (XG-1-12421-1, XL-2-02181-1, and XL-3-03147-1), Chronar has acquired considerable expertise in the preparation and purification of higher order silanes. Earlier preparation involved adding magnesium silicide to dilute acids and then purifying the silane mixture. The current method consists of first passing a very high-purity starting material (CCD grade monosilane) through a silent electric discharge (SED). By this method, electronic-grade disilane is routinely prepared. The initial mixture of silane, disilane, and trisilane produced by SED of monosilane may be separated into the constituent silanes in a series of cold traps. The disilane component is typically found by gas chromatography to be 3.9% monosilane, 95.7% disilane, and 0.3% trisilane. Films have been deposited from mainly disilane, mainly trisilane, and mixtures of all orders of higher silanes produced by this method.

1.2 DEPOSITION METHODS

Considerable research has been done on thermal CVD by static methods (principally contracts XG-1-12421-1 and XL-2-02181-1) and by flow methods (principally contracts XL-2-02181-1 and XL-3-03147-1). Flow techniques have been shown to yield higher efficiency devices. Both thermal CVD techniques, however, result in an unacceptably high density of states in the pseudo-gap.

Under this contract (XB-5-04092-1), we have been depositing hydrogenated amorphous silicon films mainly by low-pressure (a few torr) mercury-sensitized photo-CVD from higher order silanes. A serious hindrance to progress in photo-CVD has been the deposition of a highly UV absorbing a-Si:H film on the Suprasil window of the deposition chamber. It has been reported [1] that coating the inside surface of the window with certain low-vapor-pressure and UV transparent oils reduces deposition on the window. We have experimented with a large number of such oils and by this means obtained much thicker films (0.3-0.4 μm thick) and higher average growth rates (up to 0.3 A/s). In addition to the window coating, recent appropriate system modification has produced growth rates of more than 2 A/s and films as thick as 2 μm.

1.3 FILM AND DEVICE ANALYSIS

In-house analysis of the films and devices includes the following:

1. Visible and near-IR optical measurements.
2. Sub-band-gap absorption deduced from the photocurrent.
3. Room temperature dark conductivity and photoconductivity.
4. Dark conductivity as a function of temperature.
5. Photoconductivity as a function of wavelength or temperature.
6. Hole diffusion length from surface photovoltage.
7. Auger analysis.
8. SIMS analysis.
9. SEM analysis.
10. J-V curves.
11. Spectral response including light and voltage biasing.
12. Collection length.

13. Laser line scans.
14. Light-induced effects.

The first six are used principally to determine the optoelectronic properties of individual layers, while the last five are used principally to characterize completed devices. Items 7-9 for material and surface analysis, aid in the characterization of both individual layers and devices.

SECTION 2
TECHNICAL DISCUSSION

2.1 STATUS OF THERMAL CVD

Considerable work has been done to optimize both the quality of individual layers and the performance of devices prepared by both static and flow thermal CVD. Flow techniques have been shown to yield higher device efficiencies. New, wide-band-gap CVD p-layers have also been developed (see the appendix).

Single-junction device efficiencies of 3-3.5% have been achieved in all-CVD devices having a wide-band-gap p-layer. Based upon current results, we feel that even by upgrading the system and in combining the individual optimization techniques only about 4% efficiency would be achievable without further breakthroughs in the CVD technology.

The principal problem of all CVD devices is the poor quality i-layer, as measured by photoconductivity (generally less than $5x10^{-6}$ $(\Omega\text{-cm})^{-1}$ under AM1) and spin density (about 10^{17} spins/cm^3). We believe that the two main reasons for the inferior i-layers produced by thermal CVD are related to the necessarily higher deposition temperature (above 400°C for an appreciable deposition rate). First, during the deposition of the CVD film some hydrogen, which normally would cap dangling bonds, may be driven from the material because of the high deposition temperature. The loss of this hydrogen may create additional dangling bonds or neutral defects. Thus, even though the CVD films have been measured to have about 17 atomic percent hydrogen, by the nuclear reaction technique, if only a fraction of this hydrogen were lost during deposition (say 0.1%), this could produce the high defect density observed for CVD material. If this is the case, it imposes a fundamental limitation on the quality of CVD material. Second, because of the high deposition temperature, there is a greater possibility of contamination by diffusion across the substrate film interface.

2.2 TASK 1: MATERIAL PREPARATION AND ANALYSIS

For the reasons outlined in Section 2.1, we have decided to focus our attention on photo-CVD methods and in particular on the mercury-sensitized photodecomposition of disilane. In this case, mercury within the deposition chamber is resonantly excited by an external, low-pressure mercury lamp. The excited mercury can then initiate the decomposition of silane molecules. For monosilane, one of the elementary reactions is the abstraction of a hydrogen atom from monosilane, leaving SiH_3 [2]. In general the above hydrogen atom also abstracts a hydrogen atom from monosilane, forming another SiH_3 radical and molecular hydrogen. These types of reactions are also observed when starting with higher silanes [3]. Figure 1 illustrates a photo-CVD system that we have used for some of this work.

2.2.1 A-Si:H Film Growth Rate

As we mentioned, a well-known problem with photo-CVD is that deposition on the window reduces the light intensity within the deposition chamber and thereby decreases the deposition rate. Reduction in growth rate measured with the laser thickness monitor (spreading in fringe spacing) unfortunately averages over a significant deposition time. Nevertheless, using this technique in our low-growth-rate configuration, we observe nearly a threefold

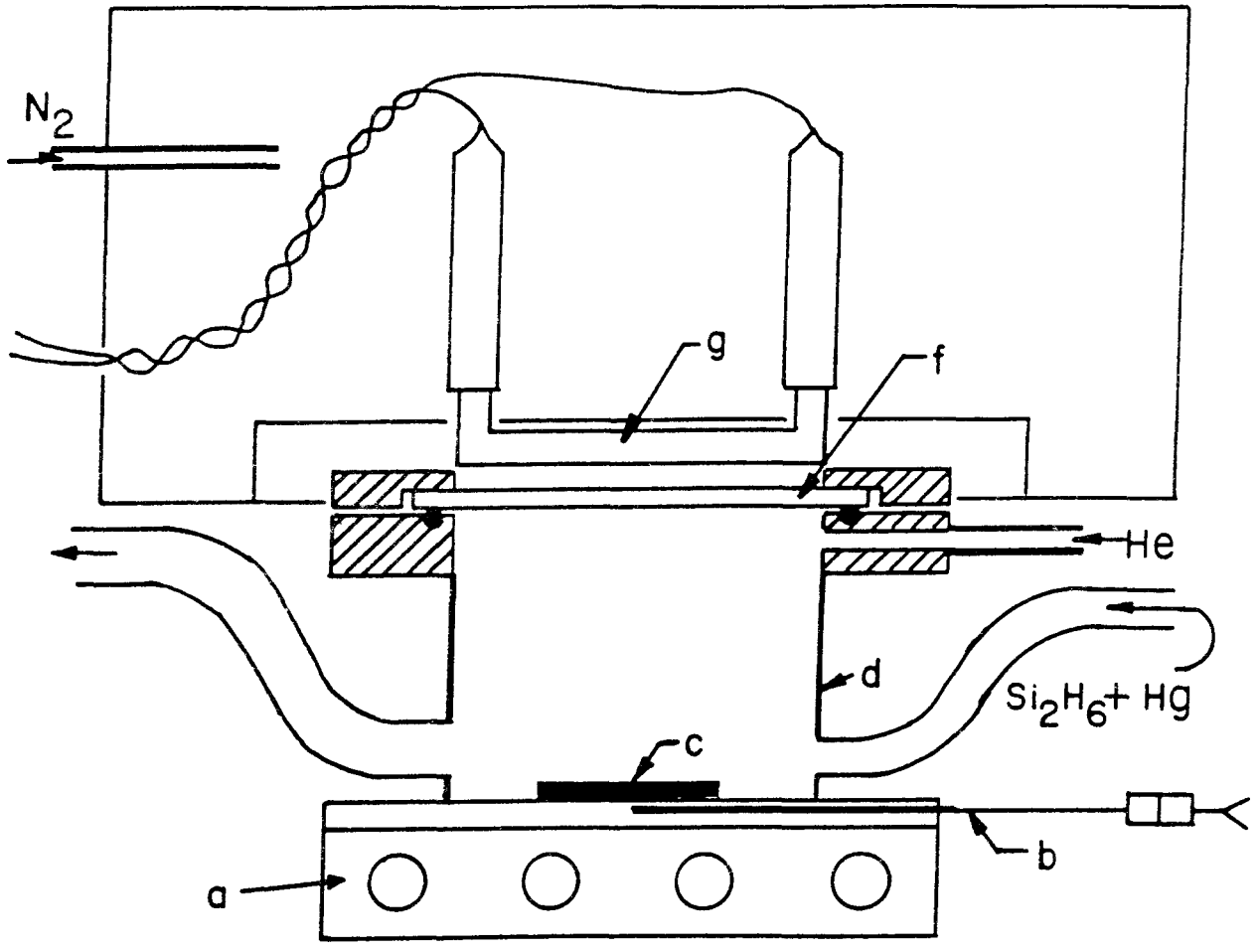

Fig. 1. Photo-CVD system (a) aluminum heater block; (b) thermocouple; (c) substrate; (d) stainless steel chamber; (f) Suprasil quartz window, and (g) low-pressure mercury lamp.

larger initial deposition rate than that observed after about 1-1/2 to 2 hours.

A simple and more accurate method for monitoring the decrease in light intensity as a function of window deposition makes use of the pressure rise in static experiments. This is expected to be proportional to the total gas-phase and deposition chemistry. These experiments are easily performed and take about 5 minutes. Results depend strongly on the initial conditions. An example of a rate of pressure rise experiment is shown in Fig. 2. The results from a set of rate of rise experiments are shown in Fig. 3. For the 90-minute deposition shown in Fig. 3, the rate of rise experiments indicate that the light intensity has fallen slightly more than a factor of three between the beginning and end of the deposition. We expect this technique to be useful in improving initial deposition rate and in decreasing the rate of fall-off in the deposition rate.

Using the rate-of-pressure-rise technique, we observe

1. That the light intensity is the same for both thin and thick low-vapor-pressure fluorocarbon window coatings indicating (a) that the oil is nonabsorbing, and (b) that a thin coating is as effective as a thick coating.

2. That the intensity of the Hg resonance radiation from the low-vapor-pressure mercury lamp is about the same for lamp temperatures of 53°C and 65°C. (The manufacturer has reported that light intensity can be sensitive to lamp temperature.)

3. That cleaning the chamber with acetone appears to reduce the maximum rate of pressure rise by over 50%. This surprising result suggests that there is residual acetone which acts as an inhibitor. However, these data should be confirmed by repeat experiments.

During these experiments, we discovered that appropriate modification of the system virtually eliminates a fall-off in the growth rate (see Fig. 4 for output from the laser thickness monitor) and improves the growth rate. This modification basically consists of reducing the substrate to window distance while using an appropriate fluorocarbon coating on the window (see below). We have not determined the upper limit to film thickness for our new deposition method. However, a film 2 μm thick was deposited for analysis by surface photovoltage. In addition, we now observe growth rates up to about 3 A/s.

The perfluoropolyether (PFPE) fluid used to date is a random copolymer of C_3F_6O and COF_2. It is manufactured by the UV stimulated photo-oxidation of hexafluoropropylene and oxygen, and is inert to a wide range of compounds. We also have experimented with fluids consisting of repeating C_3F_6O groups with CF_3 end groups. PFPE fluids may decompose if heated above 100°C in the presence of Lewis acids.

Using a sloping pedestal in the photo-CVD deposition chamber we are able to determine the a-Si:H growth rate as a function of substrate distance from the Suprasil quartz window. Figure 5 shows the result of one such experiment where the thickness of the a-Si:H i-layer was determined from the high

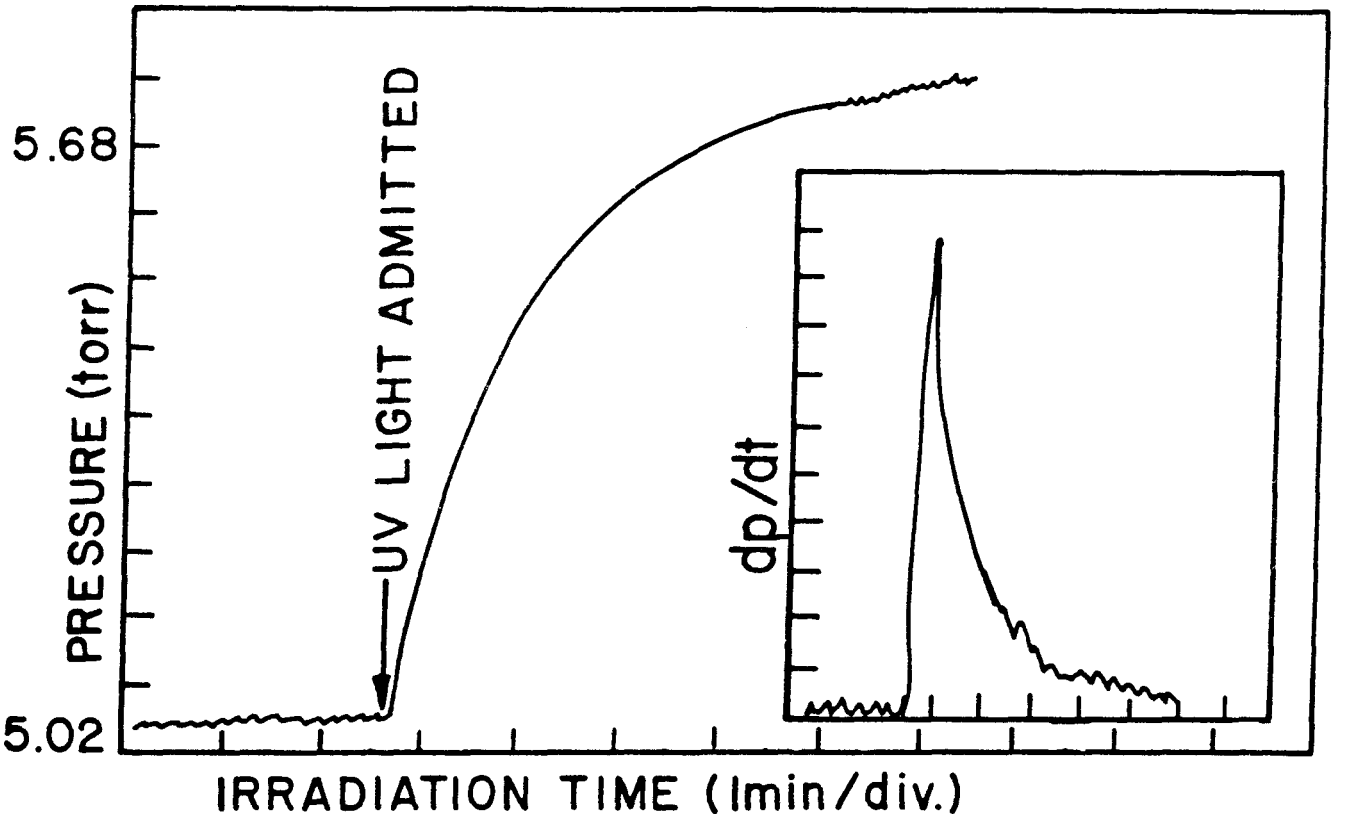

Fig. 2. Static rate of pressure rise experiment.

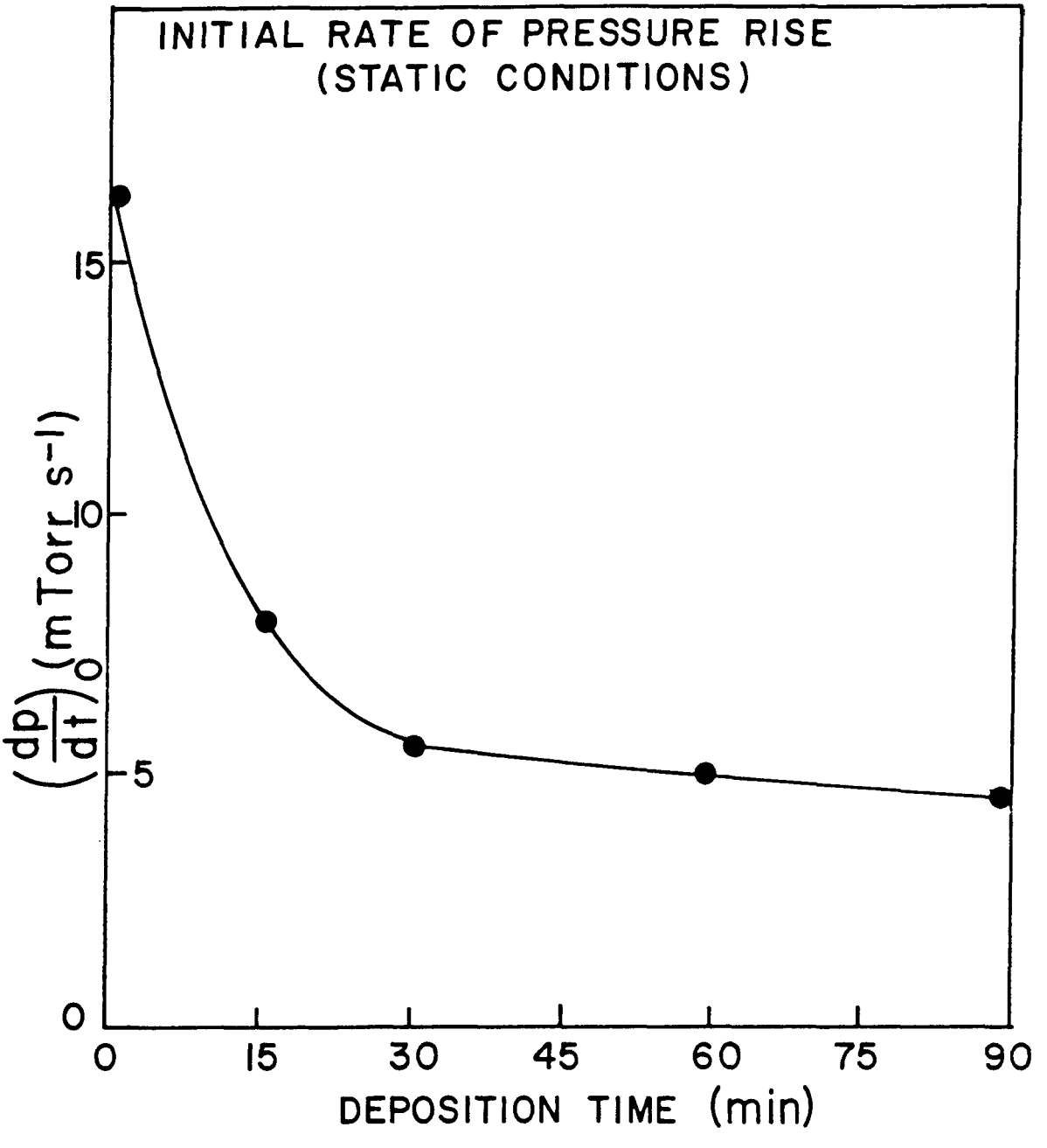

Fig. 3. The results of five static rate-of-rise experiments during a 90-minute deposition of an a-Si:H i layer by photo-CVD, showing the fall-off in the rate of pressure rise or reaction rate. The reaction rate is reduced by deposition on the quartz window which reduces the light intensity.

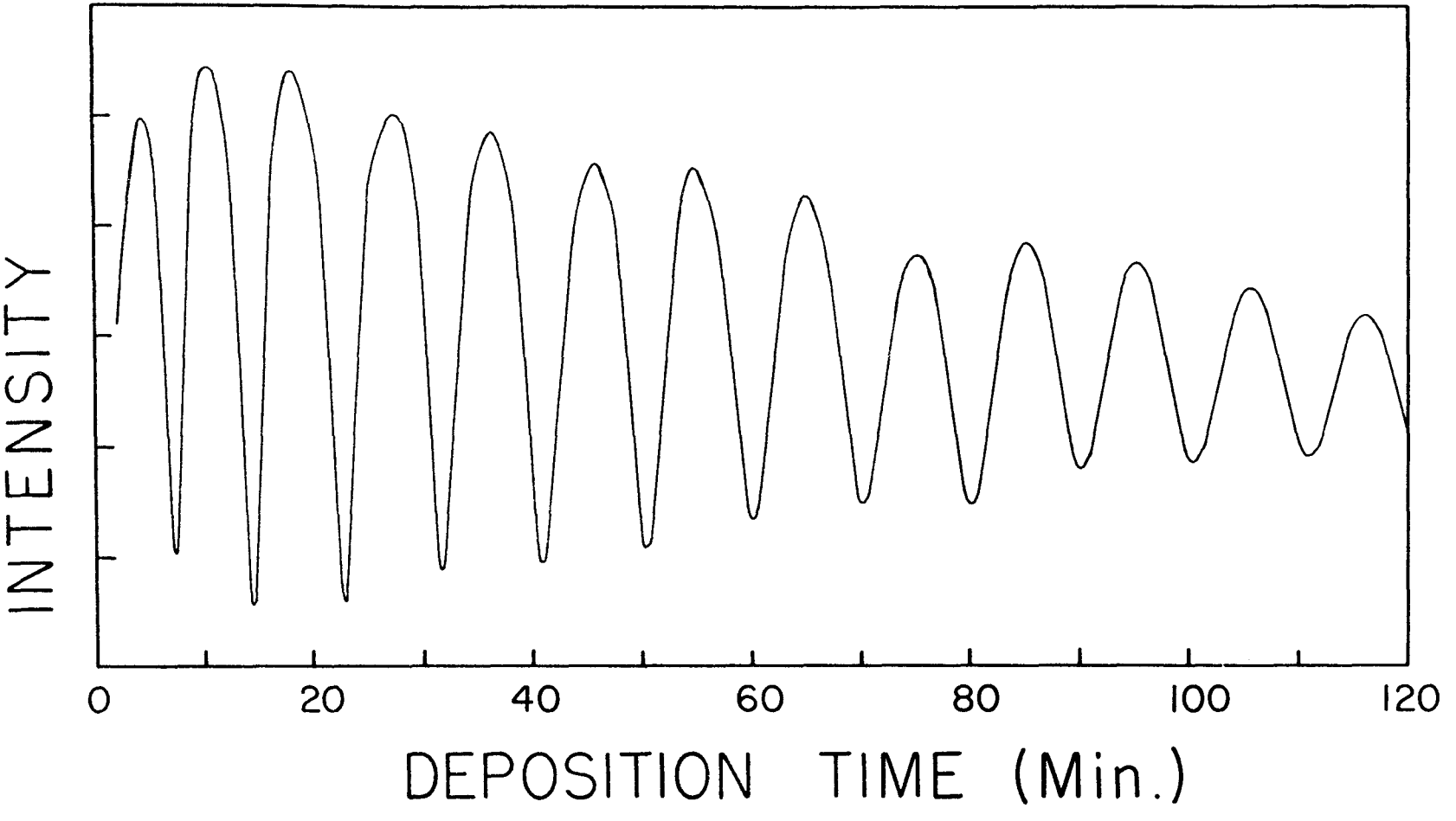

Fig. 4. Output from laser thickness monitor for photo-CVD i-layer prepared at a high deposition rate. The fringes reveal a drop in deposition rate of about 33% after 2 hours. For window-substrate spacings of 0.15 and 0.45 cm the fall-off in deposition rates after a 0.9 μm deposition were 20% and 45%, respectively.

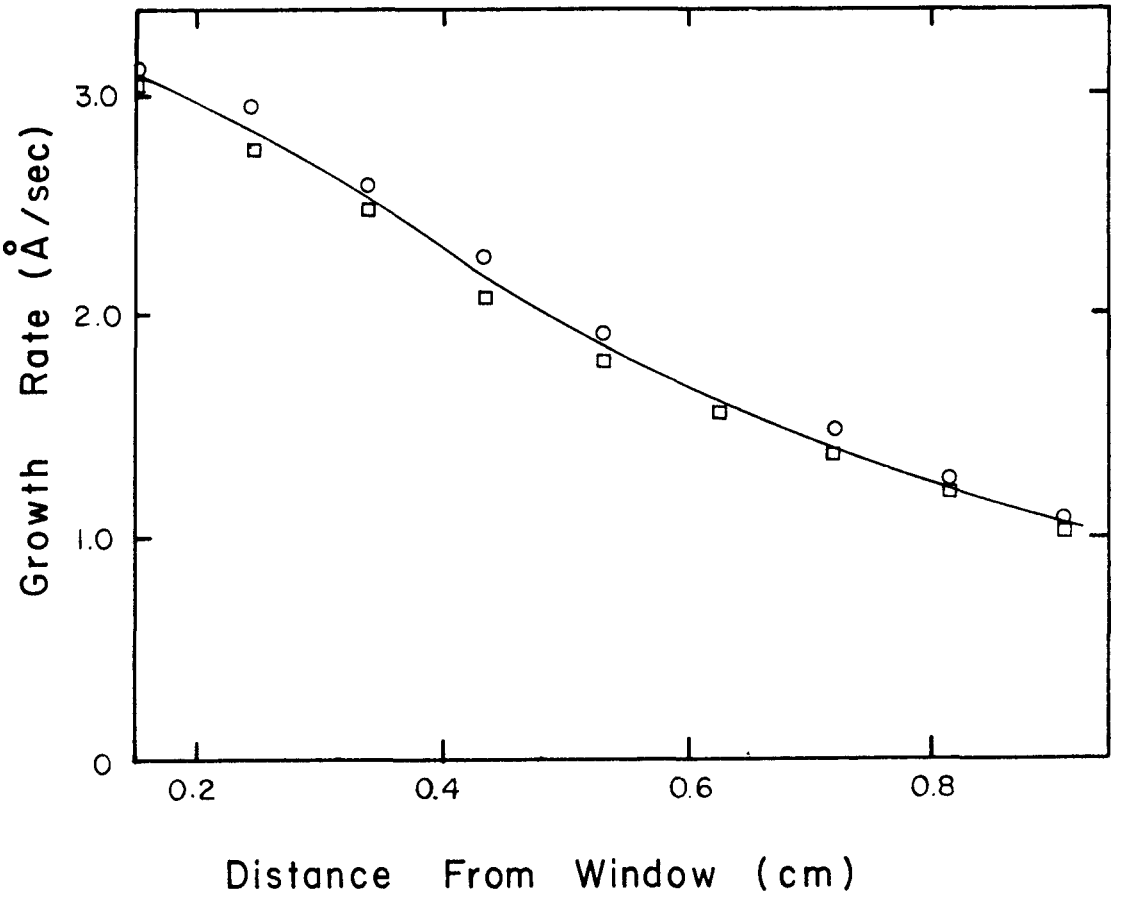

Fig. 5. Deposition rate of photo-CVD a-Si:H as a function of window-substrate separation.

frequency (100 kHz) capacitance of SnO_2/p-i-n/Al dots. A dielectric constant of 11.7 for the a-Si:H was assumed. It was also assumed that the n-layer was sufficiently conductive to not contribute to the capacitance. Over a spacing from 0.15 to 0.95 cm the growth rate decreased from about 3 to 1 A/s.

To achieve high growth rates and thicker films the temperature of the Suprasil window is higher than that for the low growth rates (the heated substrate must be closer to the window). To eliminate the possibility that a higher vapor pressure for the window oil would reduce deposition on the window, a thick film will be deposited with a cool window. Preliminary to this experiment, a 0.3-μm i-layer was deposited at a block temperature of 147°C, ensuring a cool window. The growth rate was 1.7 A/s. The optical band gap of the film is 1.87 eV and the slope of the absorption edge is 880 $(eV\ cm)^{-0.5}$.

Because of our experience with our current apparatus, we have decided to build a new reactor. In addition to permitting deposition over a larger area, it will admit a greater fraction of light from the mercury vapor lamp. From geometric factors alone, the light intensity within the chamber will increase. We expect that this will further increase the growth rate.

2.2.2 Possible Mechanism for Obtaining Thick Films

Basically, our mechanism can be explained in terms of two parallel surfaces with greatly different sticking coefficients for deposition precursors (e.g., SiH_3 radicals). The first is the substrate window which, because of the oil coating its surface, has a small sticking coefficient. The second is the substrate surface which has a large sticking coefficient (close to unity). The deposition rate on a surface is proportional to the radical concentration near the surface and the radical sticking coefficient of that surface. At the beginning of deposition, the radical concentration near the window builds up until the radical generation rate is equal to the rate of radical loss by the gas-phase chemistry (see Section 2.2.3) and by surface reactions. When the substrate is far from the window the radical concentration near the window is large and consequently, even though the sticking coefficient is small, the deposition rate on the window is relatively large. When the substrate is near the window, the equilibrium radical concentration is small, since the substrate surface serves as a radical 'sink' because of its large sticking coefficient. Consequently, the product of the radical concentration and the window sticking coefficient is small, i.e., the growth rate on the window is small. Thus, within limits determined by gas-phase chemistry and diffusion, as the substrate surface gets closer to the surface of the window, the deposition on the window decreases.

In addition to this window deposition, any particles generated in the gas phase between the window and the substrate are driven toward the window by a thermophoretic force. Particle generation is favored by a large radical concentration and an otherwise small reactant depletion rate. Both of these conditions are more likely to be obtained when the substrate is far from the window, since its presence close to the window serves to decrease the radical concentration and to deplete the reactant concentration.

2.2.3 Gas-Phase Chemistry

In the mercury-sensitized photodecomposition of monosilane or disilane, mercury within the deposition chamber is resonantly excited by an external low-vapor-pressure mercury lamp. Because the absorption cross section for resonantly exciting the mercury atoms is large, we expect a rapid fall-off in light intensity as the distance from the window increases and consequently a rapid fall-off in the concentration of excited mercury atoms. The excited mercury can then initiate the decomposition of silane molecules. For monosilane, one of the elementary reactions is the abstraction of a hydrogen atom from monosilane, leaving SiH_3 [2]. In general, that hydrogen atom also abstracts a hydrogen atom from monosilane, forming another SiH_3 radical and molecular hydrogen. These types of reactions are also observed with higher silanes [3]. In the gas phase, these radicals are depleted by reactions of the following type [4-5]:

$$2\ SiH_3 \longrightarrow SiH_2 + SiH_4 \qquad (1)$$

$$2\ SiH_3 \longrightarrow Si_2H_6^{**} \qquad (2)$$

$$Si_2H_6^{**} \longrightarrow SiH_2 + SiH_4 \qquad (3)$$

$$Si_2H_6^{**} + M \longrightarrow Si_2H_6 + M \qquad (4)$$

Reaction 1 is an example of a disproportionation reaction. The silylene (SiH_2) subsequently inserts into a silane forming a higher silane (e.g., inserting into monosilane yields disilane) or reacts with the surface. $Si_2H_6^{**}$ is an activated disilane molecule which either decomposes (reaction 3) or is deactivated by collision with another molecule (reaction 4). Analogous reactions are expected between two Si_2H_5 radicals or a Si_2H_5 radical and a SiH_3 radical except that more disproportionation and decomposition reactions are possible. These gas-phase silane reactions decrease the radical concentration and produce more complicated higher silanes. Thus, these types of reactions are consistent with the decrease in initial growth rate we observed as the substrate's distance from the window increased. In addition to this slower growth rate at a greater substrate distance, there may also be a slightly larger contribution of more complex radicals to the film growth rate (excited Hg abstraction of an H atom from a more complex silane generated by the silane gas-phase chemistry). One would expect this to lead to a poorer, less dense film. However, to date our most efficient devices have been made at large substrate distances and low growth rates.

2.2.4 I-layer Studies at a Low Growth Rate

The dark conductivity and photoconductivity of a photo-CVD i-layer were measured in a coplanar configuration as a function of temperature. The room temperature dark conductivity was 1.0×10^{-10} $(\Omega\text{-cm})^{-1}$ and the thermal activation energy was 0.71 eV. The temperature dependence of the photoconductivity, as measured with a photon flux of 8×10^{14} photons $cm^{-2}\ s^{-1}$ at 600 nm, is shown in Fig. 6. It is interesting to note that the photoconductivity exhibits a low temperature peak and thermal quenching ('Delahoy dip' or 'Vanier valley') for 1000/T between 8 and 5 (125 K to 200 K). These fea-

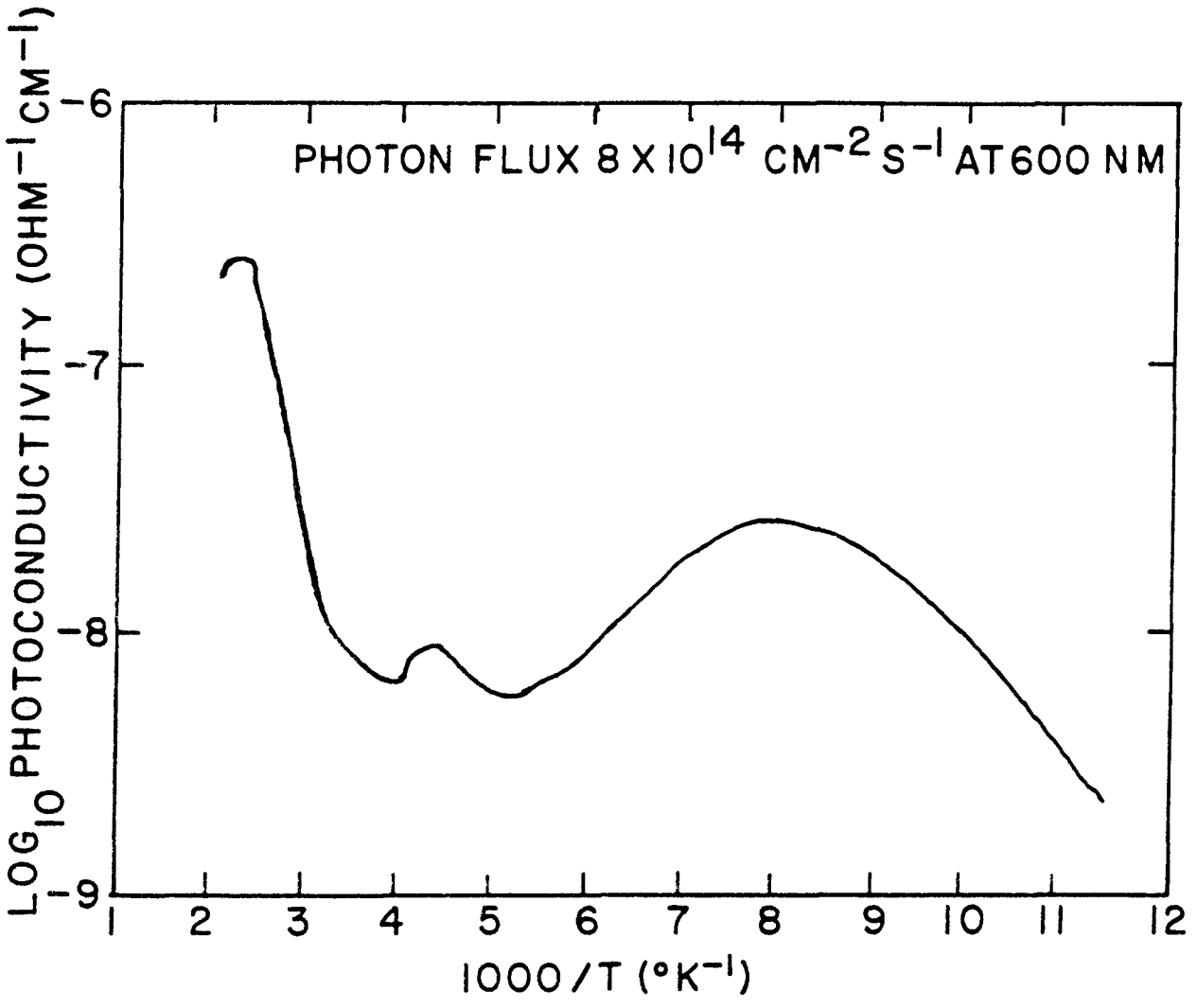

Fig. 6. Photoconductivity versus inverse temperature for a photo-CVD i-layer. Thermal quenching is observed for $5 < 1000/T < 8$.

tures are usually observed in undoped glow discharge films (and never in thermal CVD films), suggesting that photo-CVD a-Si:H possesses a gap state distribution similar to glow discharge a-Si:H. This implies the existence of two types of states in the gap, one of which is the dangling bond [6]. It is tempting to speculate that unless atomic hydrogen is present during the deposition of a-Si:H, this kind of gap state distribution does not occur. The atomic hydrogen may a) reduce the dangling bond density to allow observation of thermal quenching, and/or b) actually introduce states having a low electron capture cross section [6]. The cause of the small hump in photoconductivity that appears over a narrow temperature region near 1000/T = 4 is unknown, but it could result from surface states or reconstruction of a specific defect. A similar hump is often seen in glow-discharge films.

Representative results of the room temperature dark and AM1 photoconductivity (σ_d and σ_p) of a thin film prepared at a low deposition rate are 5.0×10^{-10} and 9.6×10^{-6} $(\Omega\text{-cm})^{-1}$, respectively. The light-to-dark ratio is 1.9×10^{4}.

2.2.5 I-layer Studies at a High Growth Rate

At high growth rates (about 1-3 A/s for disilane), a number of i-layers have been deposited and characterized by dark conductivity, photoconductivity, and optical band gap. Photoconductivities are in the range 2×10^{-3} to 2×10^{-4} $(\Omega\text{-cm})^{-1}$. The ratio of the photoconductivity to the dark conductivity is as high as 4.6×10^{5}. Of particular interest is the large difference in properties between a disilane deposition (255°C base temperature, 50°C Hg temperature, 5 torr pressure, disilane flow rate of 1.4 cm^3/min, and He flow rate of 4.5 cm^3/min) and a monosilane deposition (255°C base temperature, 50°C Hg temperature, 5 torr pressure, silane flow rate of 1.4 cm^3/min, and He flow rate of 4.5 cm^3/min). Properties for the disilane deposition were a growth rate = 1.1 A/s, $\sigma_d = 6.0 \times 10^{-8}$ $(\Omega\text{-cm})^{-1}$, $\sigma_p = 1.3 \times 10^{-3}$ $(\Omega\text{-cm})^{-1}$, $E_g = 1.76$ eV, and the slope of the absorption edge = 929 $(\text{eV-cm})^{-0.5}$. Properties for the silane deposition were a growth rate = 0.5 A/s, $\sigma_d = 7.4 \times 10^{-9}$ $(\Omega\text{-cm})^{-1}$, $\sigma_p = 5.3 \times 10^{-4}$ $(\Omega\text{-cm})^{-1}$, $E_g = 1.85$ eV, and the slope of the absorption edge = 911 $(\text{eV-cm})^{-0.5}$. The higher (almost double) growth rate for disilane was expected. However, our thermal and plasmaassisted CVD observations did not suggest the significantly larger band gap for film deposited from monosilane. We have observed that the band gap is sensitive to the substrate temperature for disilane depositions. Using the configuration for higher deposition rates originally necessitated less accurate monitoring of the substrate temperature. It is therefore possible that we were observing a temperature effect. The deposition system is being altered so that the substrate temperature can be more accurately monitored during deposition at higher growth rates. This will enable us to determine to what extent the band-gap difference is silane related. It will also contribute to the reproducibility of film deposition.

The hole diffusion length for our first 2-μm-thick sample, as determined by the constant surface photovoltage technique, is 0.27 μm (see Fig. 7). Fig. 8 shows a plot of $(\text{alpha } E)^{0.5}$ versus E for a 0.54-μm i-layer prepared under conditions similar to the 2-μm film. The band gap is 1.78 eV. The absorption coefficient for the thicker sample used in the surface photovoltage experiment was determined from the thinner sample.

A sample for ESR analysis was prepared at a substrate distance about 3

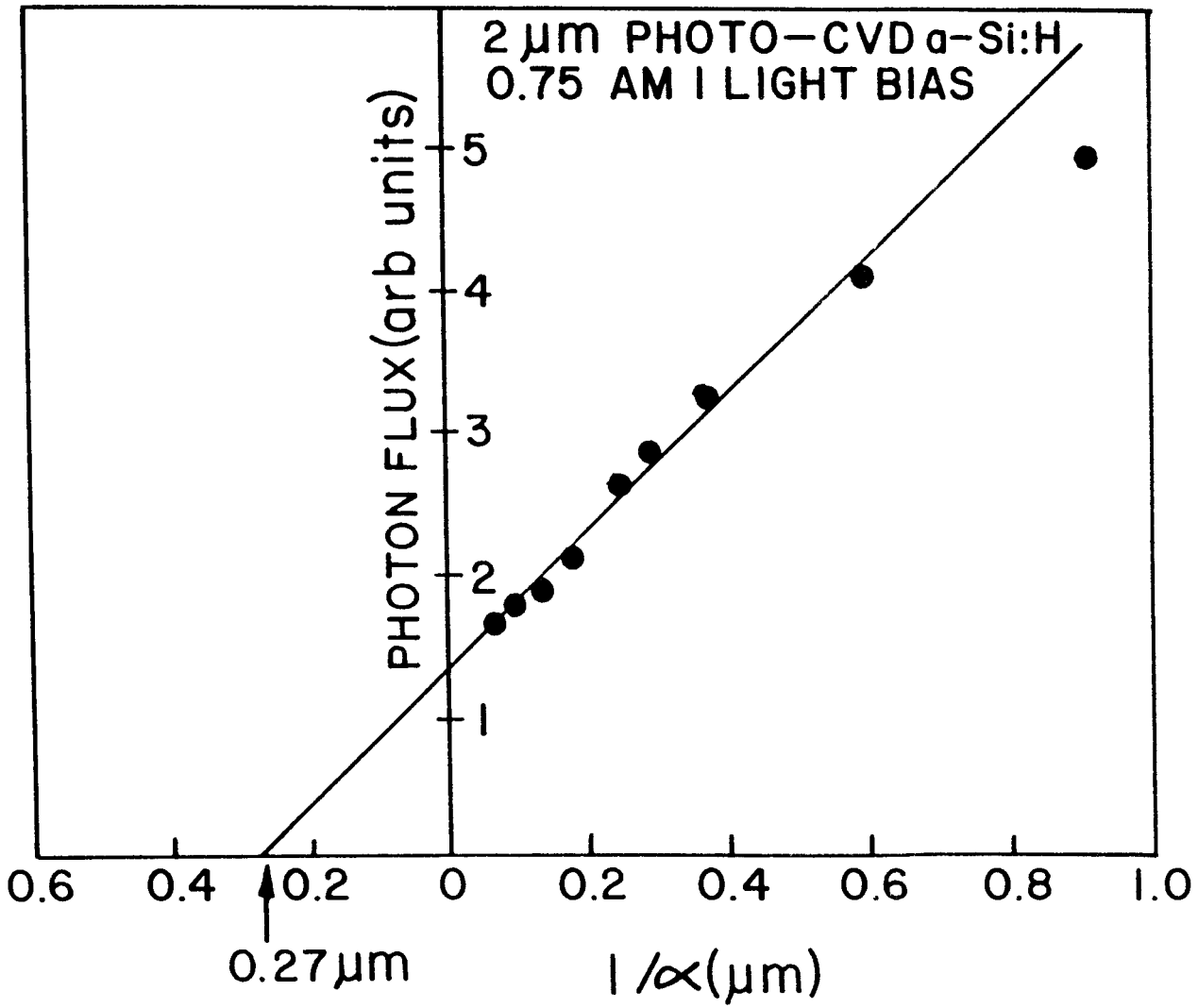

Fig. 7. Surface photovoltage measurement on 2-micron photo-CVD i-layer.

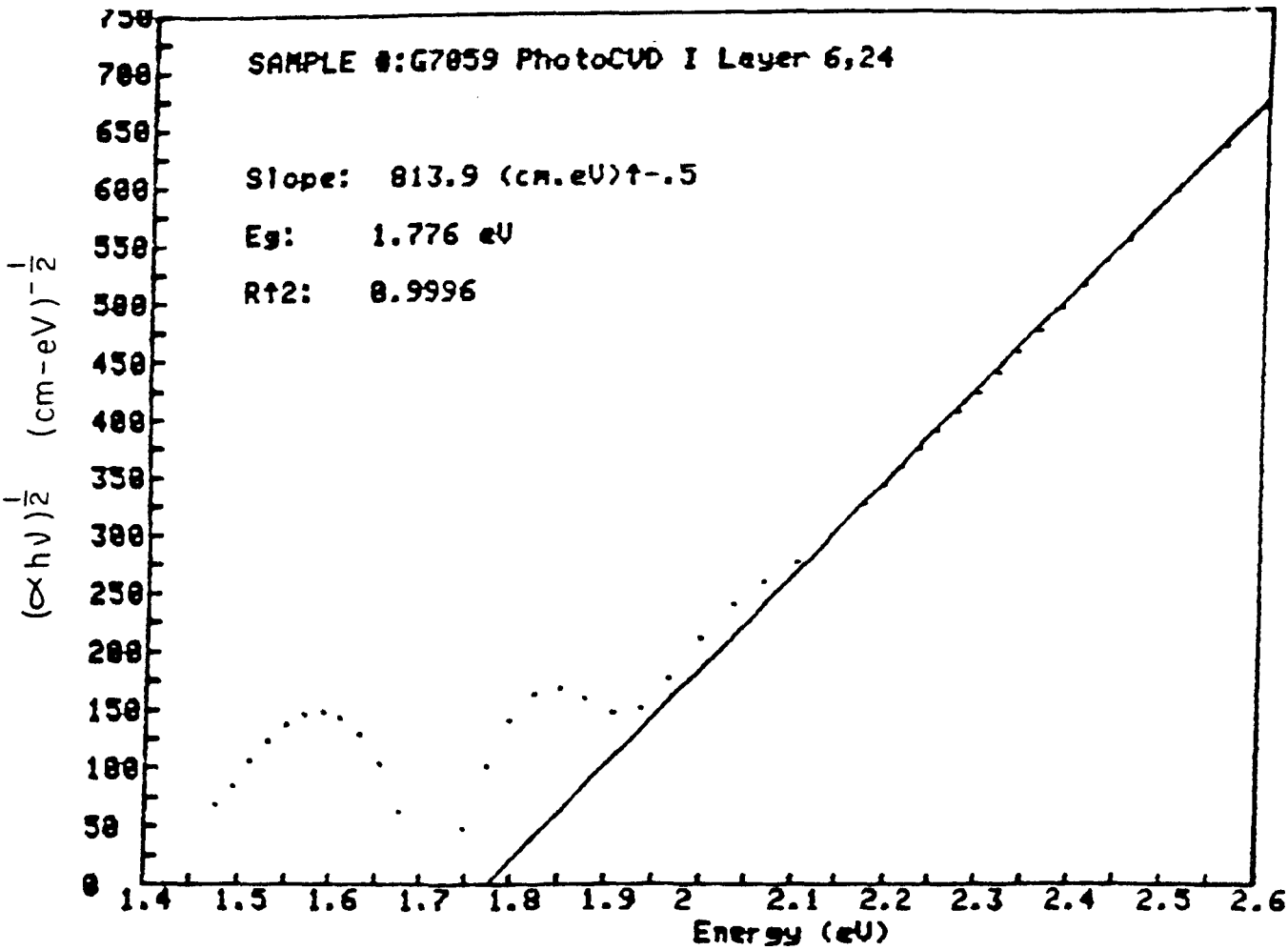

Fig. 8. Square root of the product of the absorption coefficient and the photon energy versus the photon energy for a photo-CVD i-layer.

mm greater than for the sample prepared for SPV analysis. For the sample at the slightly greater substrate distance, the initial growth rate decayed from about 2.0 A/s to about 1.1 A/s after a deposition of about 0.9 μm. This corresponds to about a 45% decrease in the growth rate. The closer sample had only about a 20% decrease in growth rate after about 0.9 μm of deposition. The ESR sample was deposited by two consecutive 2-hour depositions, each starting with a clean window. The total thickness of the sample was about 1.6 μm assuming an index of refraction of 4.2 at 630 nm. The dark conductivity is 1.2×10^{-9} $(\Omega\text{-cm})^{-1}$, the AM1 photoconductivity is 2.2×10^{-4} $(\Omega\text{-cm})^{-1}$, and the ratio of σ_p to σ_d is 1.8×10^{5}. ESR analysis indicates that the spin density is in 1×10^{16} spins per cc. This analysis shows that photo-CVD material is capable of very low spin densities.

2.2.6 P-Layer Studies at a Low Growth Rate

A new, wide-band-gap p-layer has been developed. It is deposited by the mercury-sensitized decomposition of disilane, dimethylsilane, and diborane. For example, using equal mixtures of disilane and dimethylsilane and a diborane-to-total-silane ratio of 0.3%, we obtain a p-layer with the following properties: a band gap of 1.97 eV (see Fig. 9) and a dark conductivity of 7×10^{-6} $(\Omega\text{-cm})^{-1}$. Omission of the dimethylsilane yields a p-layer with a gap of 1.66 eV.

A J-V curve of a p-i-n device where the a-Si:H layers were deposited using mercury-sensitized photodecomposition of disilane is shown in Fig. 10. The device has a wide-band-gap silicon-carbide p-layer and a conversion efficiency of 5.8%. When a similar device was fabricated with the mercury lamp turned off during the p-layer deposition, the V_{oc} was only 0.44 V, which shows that the the p-layer is photochemically, and not thermally, derived.

2.2.7 N- and P-Layer Studies at a High Growth Rate

Optimal deposition conditions for devices deposited at high growth rates appear to be considerably different from those for low growth rates. Tables I and II show the properties of some n- and p-layers deposited approximately 2 mm from the quartz window. The maximum dark conductivity of an n-layer in this study is 5.2×10^{-3} $(\Omega\text{-cm})^{-1}$. This film was deposited at 2.8 A/s. It is worth noting that helium dilution decreases the growth rate and hydrogen dilution appears to increase it. The p-layer for run 69A has a band gap of 1.93 eV and a dark conductivity of 8.7×10^{-7} $(\Omega\text{-cm})^{-1}$. Both the band gap and conductivity of the p-layer need to be increased for optimal device performance.

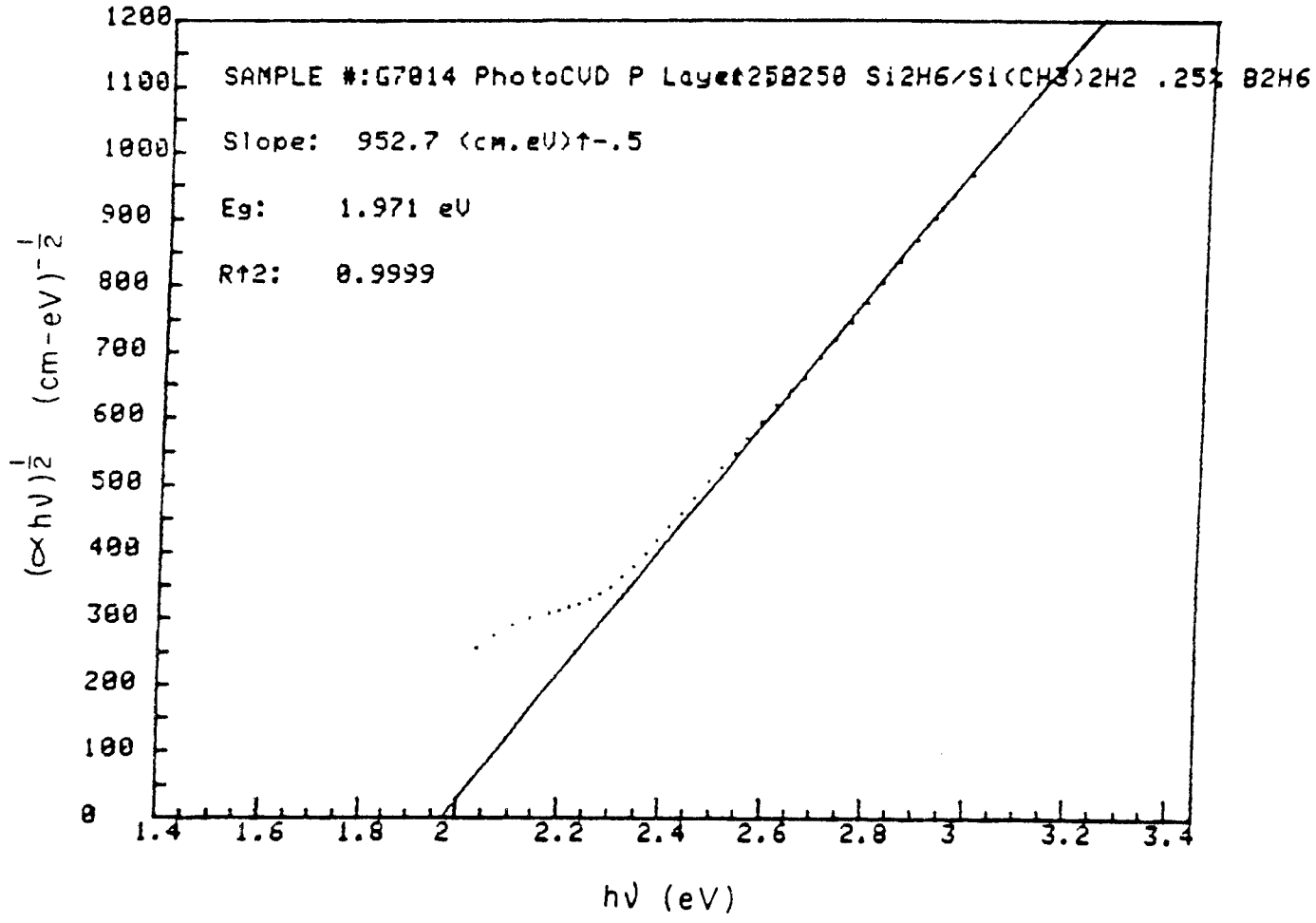

Fig. 9. Square root of the product of the absorption coefficient and the photon energy versus the photon energy for a photo-CVD p-layer.

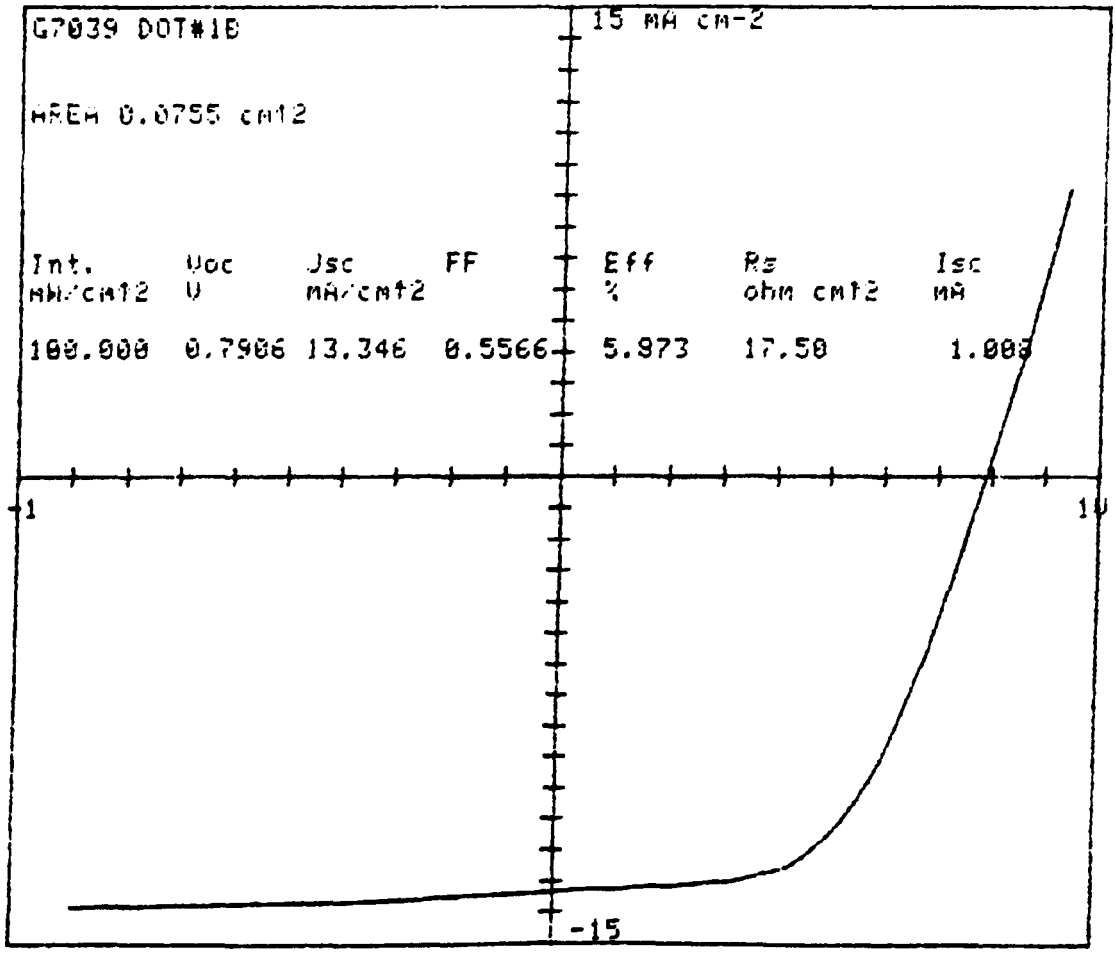

Fig. 10. J-V curve for a photo-CVD device with a wide-band-gap p-layer.

TABLE I. N-layer deposition conditions and properties for a substrate-to-window spacing of approximately 2 mm. In each case the heater block temperature was 240°C, the mercury reservoir temperature was 50°C, and the deposition pressure was 5 torr.

Sample No.	Si_2H_6 (F.M.U.)	10% PH_3 in Ar (sccm)	He (sccm)	H_2 (sccm)	Growth Rate (A/s)	σ_d $(\Omega\text{-cm})^{-1}$	E_g (eV)	Slope $(eV\text{-cm})^{-0.5}$
67A	10	1	15	0		8×10^{-4}*		
67C	10	1	15	0	2.3	3.7×10^{-3}	1.77	835
68B	9	4	0	80	2.8	5.2×10^{-3}	1.77	806
68A	9	4	80	0	1.2	4.2×10^{-3}	1.73	606
67B	8.5	4	180	4	<0.3**	$>2\times10^{-6}$		

*Thin film (growth rate for sample 67C assumed).
**Thin film (thickness estimated).

TABLE II. P-layer deposition conditions and properties for a substrate-to-window spacing of approximately 2 mm. In each case the heater block temperature was 240°C, the mercury reservoir temperature was 50°C, and the deposition pressure was 5 torr.

Sample No.	Si_2H_6 (F.M.U.)	$SiMe_2H_2$ (F.M.U.)	2% B_2H_6 in H_2 (sccm)	He (sccm)	Growth Rate (A/s)	σ_d $(\Omega\text{-cm})^{-1}$	E_g (eV)	Slope $(eV\text{-cm})^{-0.5}$
69A	3.5	2	1	20	1.6	8.7×10^{-7}	1.93	845
69B	6.5+1	9	1	180	<0.2*	$>10^{-9}$		

*Thin film (thickness estimated).

2.3 TASK 2: DEVICE FABRICATION AND ANALYSIS

The basic device structure is glass/SnO_2/p-i-n/Al. In our previous work an efficiency of 4.4% and a current density of 10 mA/cm^2 were achieved under AM1 illumination. In the current work the best efficiency is 6% (after annealing at about 80°C to improve metallization n-layer contact) and the maximum current density exceeds 13 mA/cm^2.

2.3.1 Optimization Study

The control p-i-n device is 4.6% efficient. This optimization included

varying the concentration of the diborane and the deposition time for the wide-band-gap p-layer made from disilane and dimethylsilane, increasing the i-layer thickness, and increasing the n-layer thickness and phosphorous doping level. Increasing the n-layer thickness improved the V_{oc} from about 0.65-0.70 V to about 0.73-0.74 V. Increasing the phosphorous concentration in the n-layer yielded no further improvement in the V_{oc}. In this study, optimization of the p-layer alone had little effect on the V_{oc} but affected the fill factor by over 10% and the I_{sc} by slightly less than 10%. This study led to about a 20% improvement in device efficiency or to a 5.5% efficient device. The I-V curve for this device, G7028, is shown in Fig. 11. It has a V_{oc} of 0.73 V, a J_{sc} of 11.5 mA/cm^2, and a fill factor of 0.66.

2.3.2 Tin Oxide

In an effort to improve the short-circuit current density, we conducted a brief study using large-grained or milky tin oxide. Although there was a marginal gain in current density, the large loss in fill factor and the loss in V_{oc} indicated that this tin oxide decreased the device shunt resistance by partial shorting through the a-Si:H between the aluminum and the tin oxide. The importance of light trapping in achieving high efficiency solar cells is well known. Therefore, much research is being done to obtain appropriate large-grain tin oxide by several different techniques.

2.3.3 The P-Layer/I-layer Interface

To improve the V_{oc} and the current density, several experiments have been performed to alter the p-layer/i-layer interface. The I-V curve for the first experiment is shown in Fig. 12. The photovoltaic parameters are an efficiency of 5.5%, a V_{oc} of 0.79 V, a J_{sc} of 11.7 mA/cm^2, and a FF of 0.60. One notes that there is a substantial improvement in V_{oc}. However, there is also some loss in the fill factor. Further work led to an increase in J_{sc} to 13.4 mA/cm^2.

2.3.4 Quantum Efficiency Plots

Routine device analysis includes spectral response and plots of quantum efficiency. The analysis includes unbiased spectral response and biased (both light and forward and reverse applied voltage) spectral response data. An illustrative example is provided in Fig. 13 where two different quantum efficiency curves for device G7017 are shown. We observe that reverse biasing has little effect on the spectral response. The small gain in area under curve B compared to curve A, shows that most of the photogenerated carriers are collected. The flatness of the ratio of curve A to curve B shows that electron and hole transport are comparable.

2.3.5 SIMS Analysis of P-I-N Device

A SIMS depth profile for a photo-CVD p-i-n cell (no carbon in the p-layer) is shown in Fig. 14. A sharp p/i interface with the suggestion of a 0.05 μm wide boron shoulder is revealed. Dissociation of the tin oxide is not apparent.

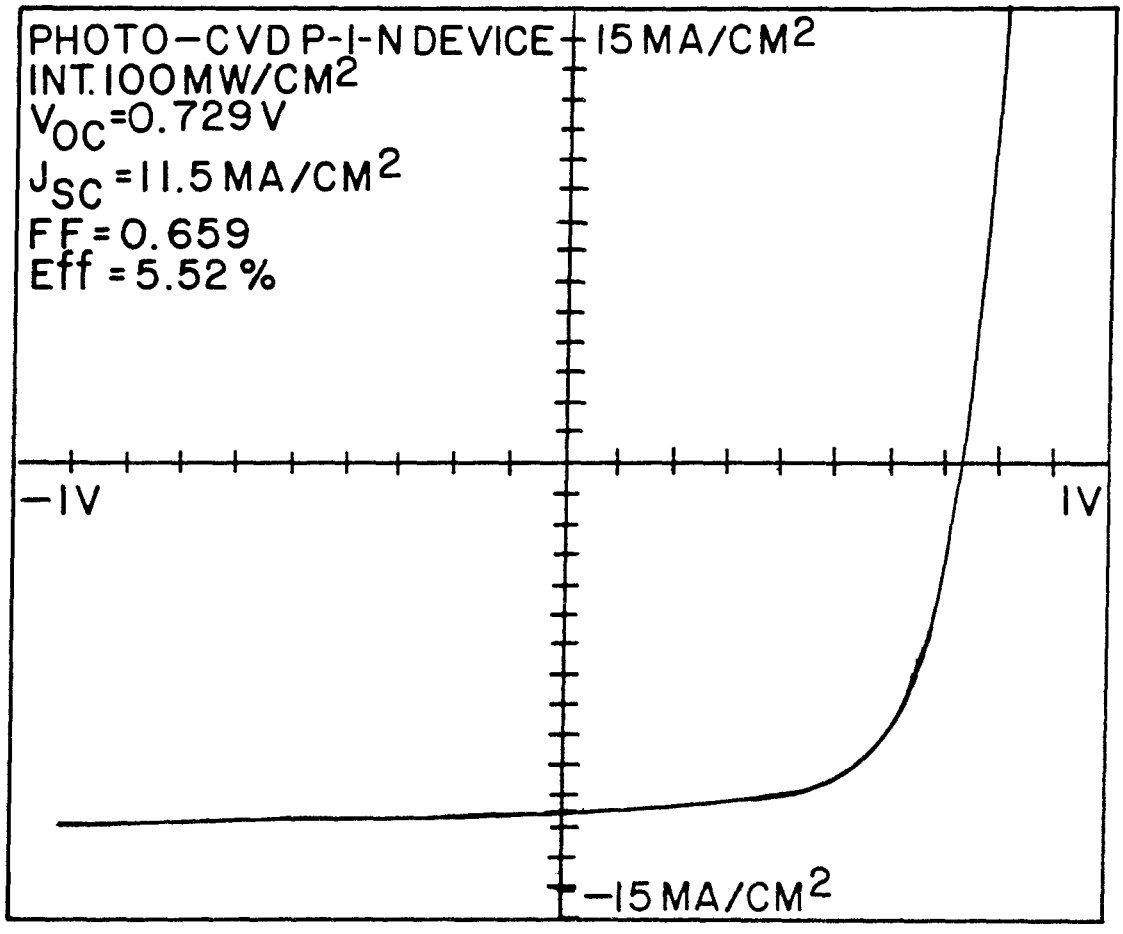

Fig. 11. J-V curve for a photo-CVD device.

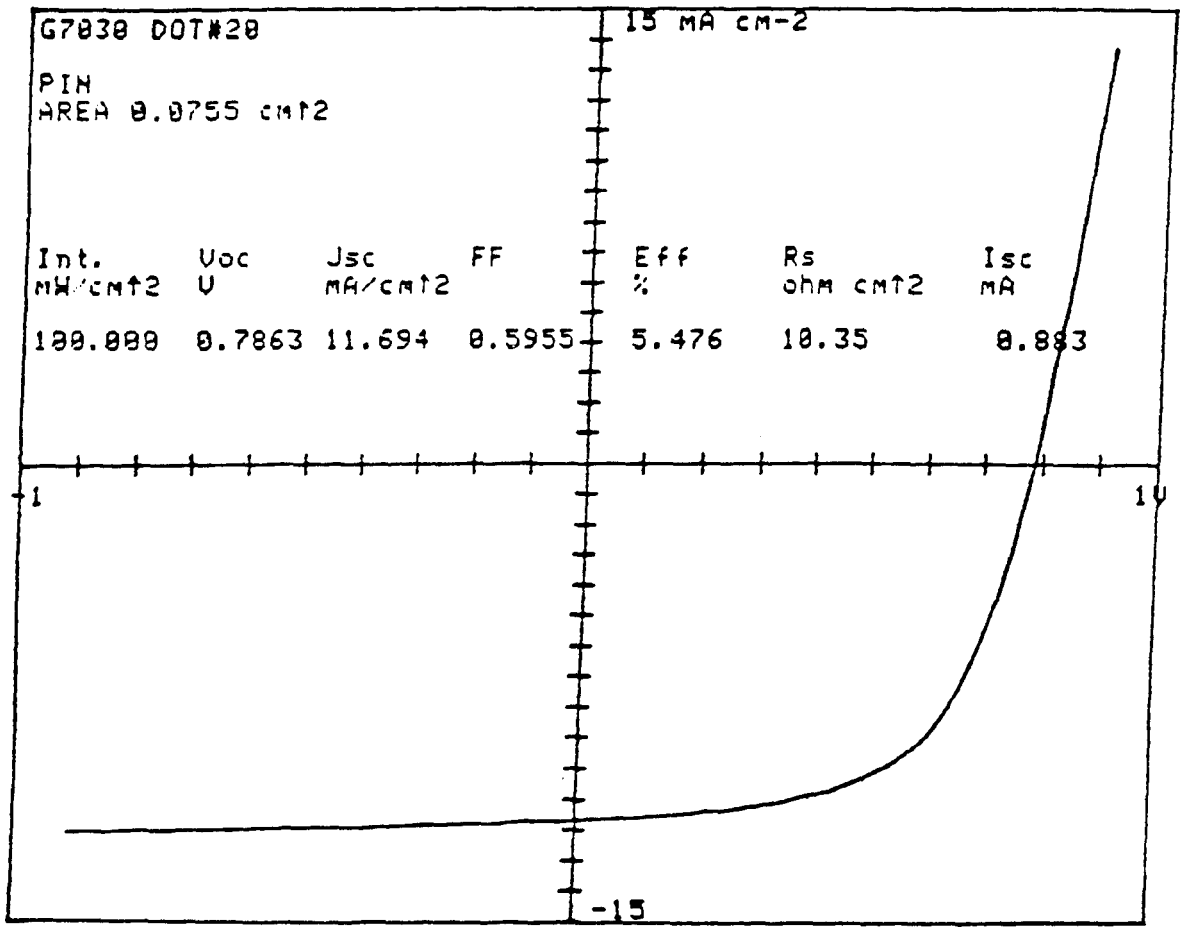

Fig. 12. J-V curve for a photo-CVD device.

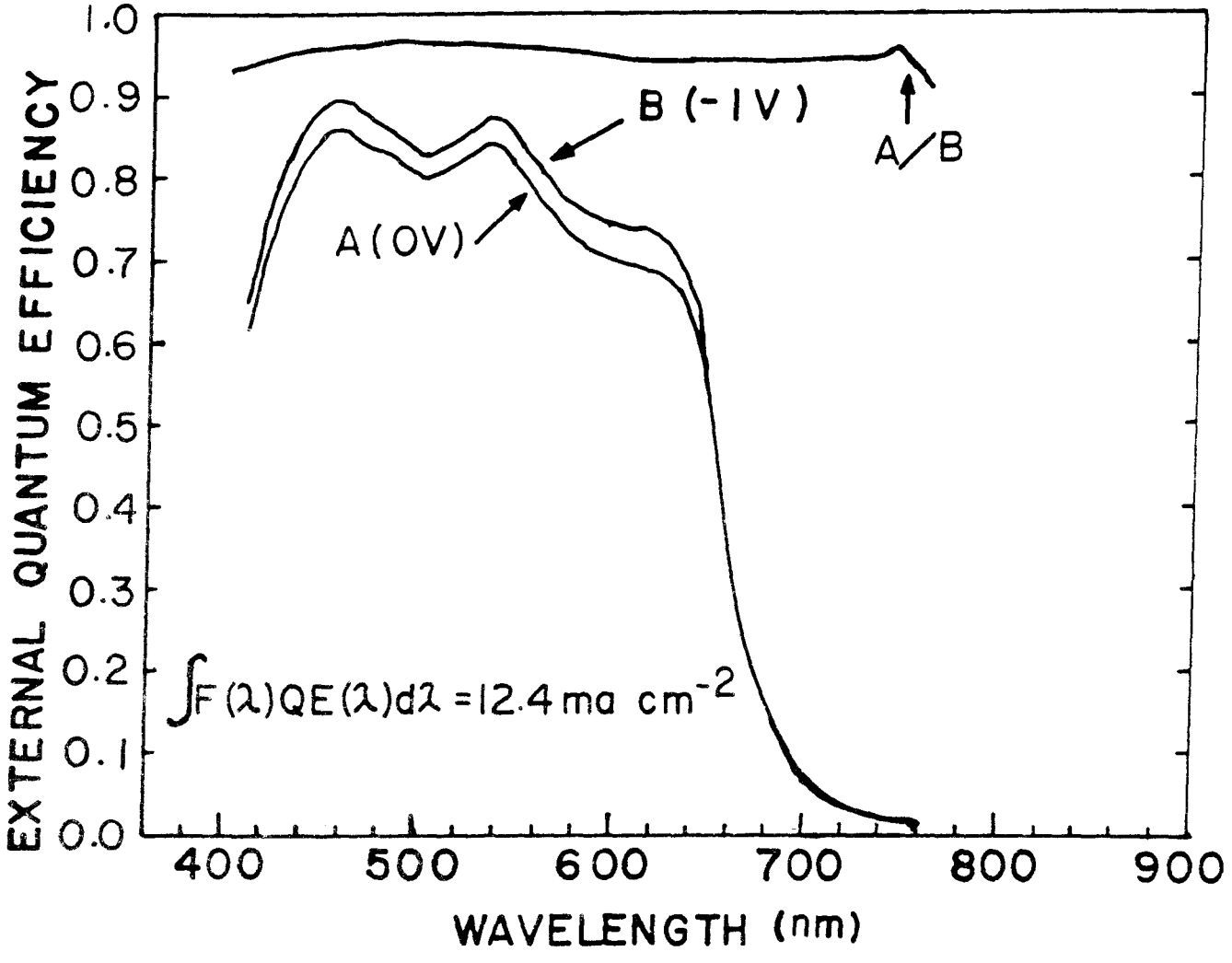

Fig. 13. Quantum efficiency plots for a photo-CVD device. Curve (A) - unbiased; curve (B) - reverse biased by one volt.

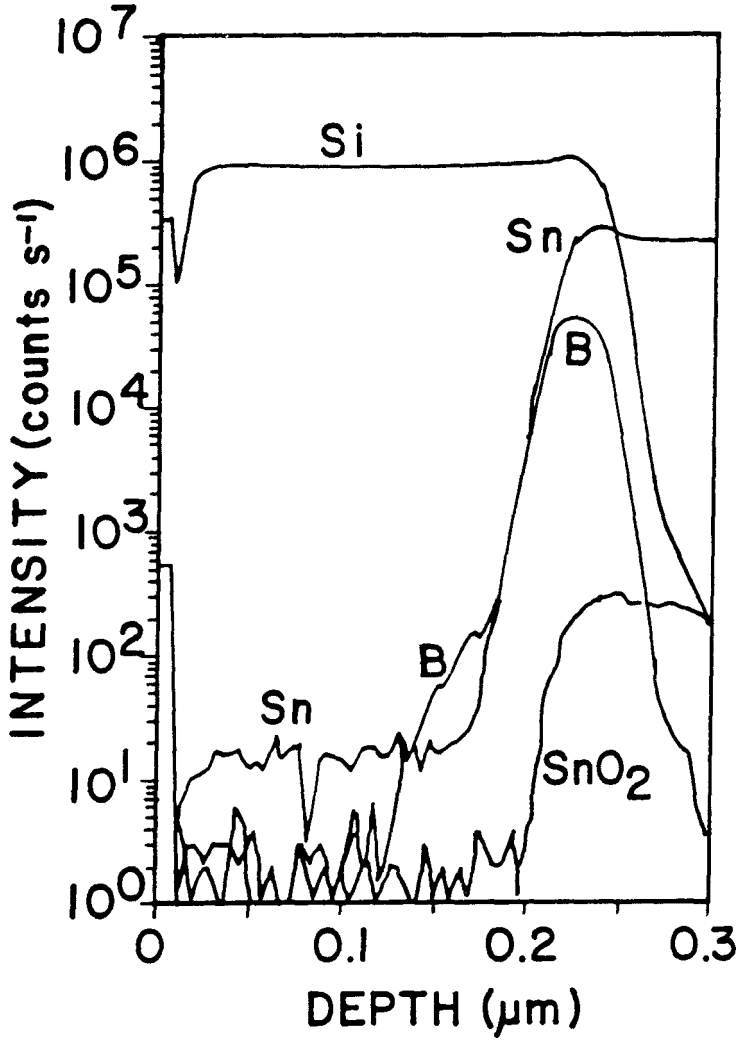

Fig. 14. Depth profile obtained by SIMS of Si, B, Sn, and SnO_2 for a 4.4% efficient photo-CVD p-i-n device.

2.3.6 P-I-N Devices Deposited at a High Growth Rate

Unfortunately, although the devices fabricated at the high growth rate often exhibit large open-circuit voltages (0.85 to 0.95 V), they have poor short-circuit current densities and fill factors. The best device deposited at a high growth rate, G7059A, had a 32-minute i-layer (previously, at low growth rates 3-hour i-layers were typical). Under simulated AM1 illumination, the efficiency is 3.9%, V_{oc} is 0.83 V, J_{sc} is 11.3 mA/cm^2, and the fill factor is 0.41.

The SPV and ESR results on the i-layers deposited at high growth rates indicate that this material could produce much higher efficiencies. However, neither measurement is definitive since SPV results appear to be spurious if the sample is slightly p type and ESR results can be misleading if there is a significant spinless defect concentration. Nevertheless, considering these measurements as well as the high photoconductivy, a high quality i-layer material appears to be possible. The poor device results could stem from poor p- or n-layers as well as associated interfaces. In addition, using IR absorption measurements on a film deposited at a high growth rate, SERI has observed significant (on the order of a percent or more) oxygen contamination. (In Section 2.5, the recently obtained results for IR, ESR, and luminescence measurements are discussed in more detail.)

2.3.7 Light-Induced Effects

The Staebler-Wronski effect is observed in photo-CVD material. A-Si:H i-layer G7058 initially had a dark conductivity of 6.4×10^{-10} $(\Omega\text{-cm})^{-1}$ and a photoconductivity of 1.8×10^{-4} $(\Omega\text{-cm})^{-1}$. After 14.5 hours illumination at AM1 the dark and photoconductivity were, respectively, 8.3×10^{-11} and 9.5×10^{-6} $(\Omega\text{-cm})^{-1}$. The dark conductivity decreased by about a factor of 8 while the photoconductivity decreased by about a factor of 19, indicating that this photo-CVD sample exhibits the Staebler-Wronski effect.

The efficiencies of two p-i-n cells from sample G7025 were measured. The sample was then annealed and the efficiencies were remeasured. These efficiencies are used as the initial ones. The sample was light-soaked at AM1 and 29°C for 2 hours. One cell degraded in efficiency by 4.5% and the other by 2.1%. The data for this study are found in Table III. Also included in Table III are the results of successive low-temperature annealings. These show that even at 85°C most of the lost cell efficiency is recovered after 1-2 hours. Parenthetically, we note that this degradation is about a factor of two less than what is often observed in devices produced by glow-discharge methods. However, because of the sparseness of the data and since the i-layer is thinner for the photo-CVD devices, we cannot conclude that they exhibit less light-induced degradation.

Another light-soaking study was undertaken using laser light. As before, care was taken to ensure that the sample started in the unsoaked state. On an x,y table the sample was scanned for 15 minutes using approximately 40 AM1 red laser light. The results are shown in Table IV. The brief laser light-soaking produced about 5% degradation in the cell efficiency. In other words, it is roughly equivalent to the 2-hour AM1 light soaking.

Table III. Photo-CVD AM1 light soak and low temperature anneal. Two dots were measured,annealed, AM1 light soaked, and annealed again.

G7025		Voc (V)	Jsc (ma/cm^2)	FF	η
Initial	Dot#2	0.7293	13.157	0.6269	6.015
	Dot#4	0.7459	13.154	0.5847	5.737
85 C, 2.5 hrs					
	Dot#2	0.7275	13.092	0.6333	6.032
	Dot#4	0.7240	13.200	0.5979	5.714
AM1 soak	Dot#2	0.7189	12.921	0.6200	5.759
29 C, 2hrs	Dot#4	0.7354	12.955	0.5871	5.593
85 C, 1 hr	Dot#2	0.7307	12.837	0.6271	5.882
	Dot#4	0.7341	12.932	0.5975	5.672
85 C, 2hrs	Dot#2	0.7526	12.770	0.6172	5.931
	Dot#4	0.7523	12.937	0.5775	5.621
85 C, 3hrs	Dot#2	0.7440	12.749	0.6223	5.903
	Dot#4	0.7458	12.937	0.5892	5.685
85 C, 4hrs	Dot#2	0.7350	12.997	0.6217	5.939
	Dot#4	0.7362	13.004	0.5886	5.635

Table IV. Photo-CVD laser soak and low temperature anneal. A dot was measured, annealed, laser soaked, and annealed again.

G7024 Dot #5	Voc (V)	Jsc (ma/cm^2)	FF	η
Initial	0.7587	13.157	0.5124	5.115
85 C, 2.5hrs	0.7409	13.209	0.5276	5.164
Laser soak	0.7536	12.832	0.5047	4.881
85 C, 1hr	0.7589	12.962	0.5084	5.001
85 C, 2hr	0.7519	12.944	0.5256	5.115

2.4 TASK 3: NON-SEMICONDUCTOR MATERIALS RESEARCH

In photo-CVD and GD deposition of silanes our most efficient devices are deposited below 250°C. In the thermal CVD of higher silanes in the temperature range of about 440-470°C, we have observed a rapid degradation (reduction) of the tin oxide by the strongly reducing silane environment. A study was undertaken to determine if less efficient photo-CVD and GD devices were produced at higher temperatures, at least in part, because of the interaction between the tin oxide and the depositing silicon film.

Four samples were deposited on tin oxide with the typical silicon-carbon p-layer followed by approximately 400 A of i-layer by glow discharge deposition at 175°, 200°, 325°, and 375°C. In each case, 30 minutes after the deposition was completed the films were removed from the deposition chamber. The interaction between the a-Si:H and the tin oxide was then characterized by Auger and SIMS analysis. Surprisingly, no trend was observed between the deposition temperature and the broadness of the interface. In fact, all films exhibited sharp interfaces (see Figs. 15 and 16, which show the Auger analysis of the low- and high-temperature films). In all cases the tin concentration in the bulk of the i-layer was below the SIMS detection limit (see, for example, Fig. 17). The SIMS data did reveal that the atomic hydrogen concentration decreased from about 30% to about 5% as the temperature increased from 175° to 375°C without otherwise altering the deposition conditions. It is not known how representative the Chronar tin oxide used in this study is compared to tin oxide deposited by other means or under other conditions. However, this study indicates that interaction between tin oxide and the depositing silicon film is not necessarily a problem below 375°C.

2.5 RECENT RESULTS: IR, ESR, AND LUMINESCENCE MEASUREMENTS

An infra-red transmission spectrum of an a-Si:H film prepared in the high-deposition-rate mode on crystalline Si at about 180 °C is shown in Fig. 18. The predominant bands are the SiH bending and stretching modes at 640 cm^{-1} and 2000 cm^{-1}. Very weak bands due to $(SiH_2)_n$ are also seen at 845 cm^{-1} and 890 cm^{-1}. On the order of a percent oxygen contamination is evident in this sample from the broad band centered at 985 cm^{-1}. Films grown in the low rate mode are known to have much less oxygen contamination (only $2x10^{19}$ oxygen atoms/cm^3). In the present case the oxygen is believed to originate from partial decomposition of the window oil. Since the window can reach 120 °C we are investigating whether the oil is degraded thermally, photolytically, or by radical attack.

Luminescence spectra using a cooled Ge detector were obtained at 6 °K using a chopped 5145 angstrom beam incident on 1 μm a-Si:H deposited on a sandblasted SiO_2 substrate. A typical spectrum is shown in Fig. 19, normalized for system response, and plotted as intensity per unit energy. A single intense emission band at 1.38 eV is observed with a full width at half height of 296 meV. The quantum efficiency was found to be slightly higher than the best glow discharge a-Si:H sample examined, implying a low density of dangling bonds. However, the peak width is somewhat larger than for some glow discharge films and may indicate broader band tails.

ESR measurements were performed at 10 °K at low microwave powers on photo-CVD a-Si:H deposited on Suprasil quartz cover slips. The g value was 2.0053 (Si dangling bonds) and careful integration under the line yielded a spin density of $1x10^{16}$ cm^{-3}.

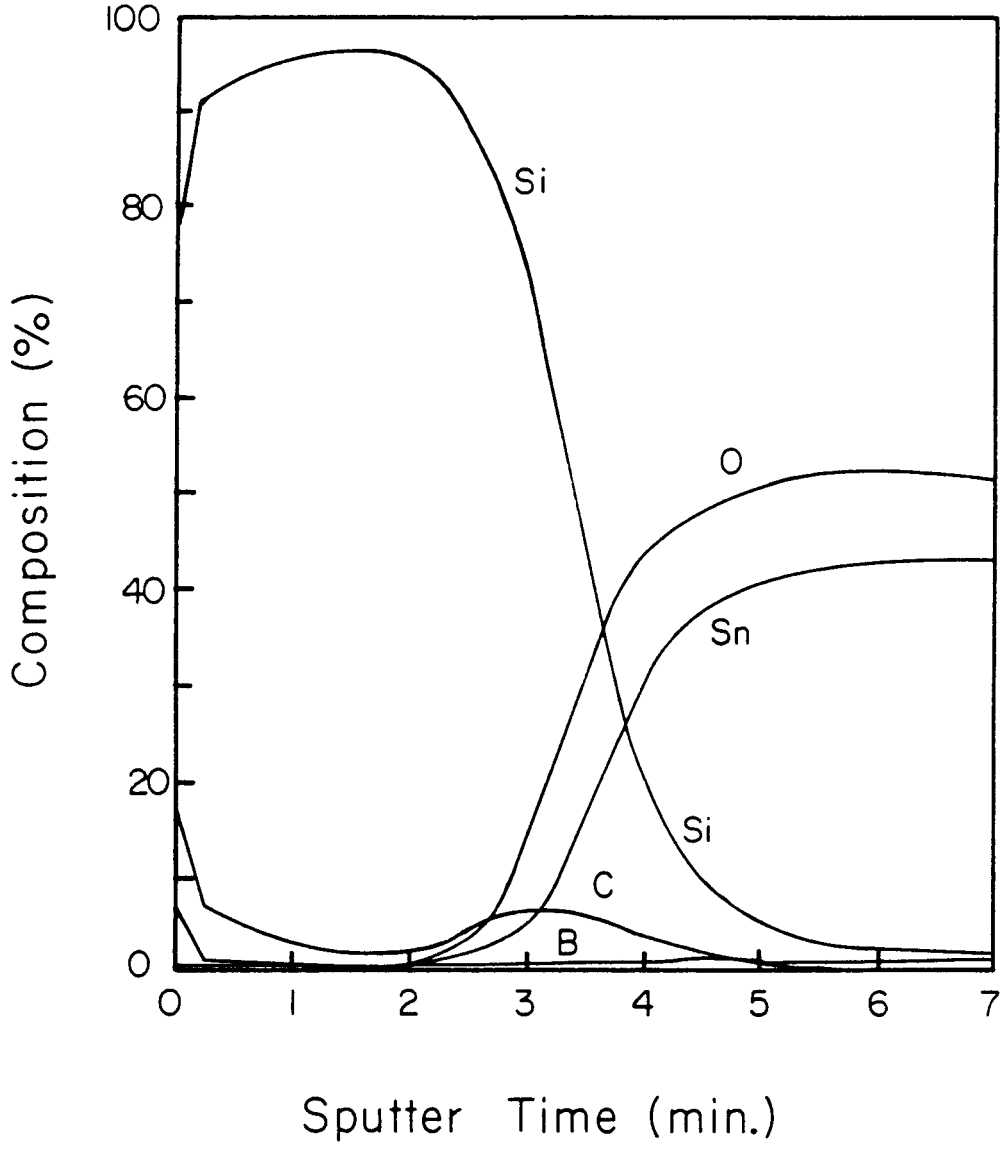

Fig. 15. Auger depth profile of ~400 A i a-Si:H/100 A p a-Si_xC_{1-x}/SnO_2/glass where amorphous silicon and silicon-carbide layers were prepared at 175 C. Tin is in the elemental state for sputtering time less than about 3 minutes.

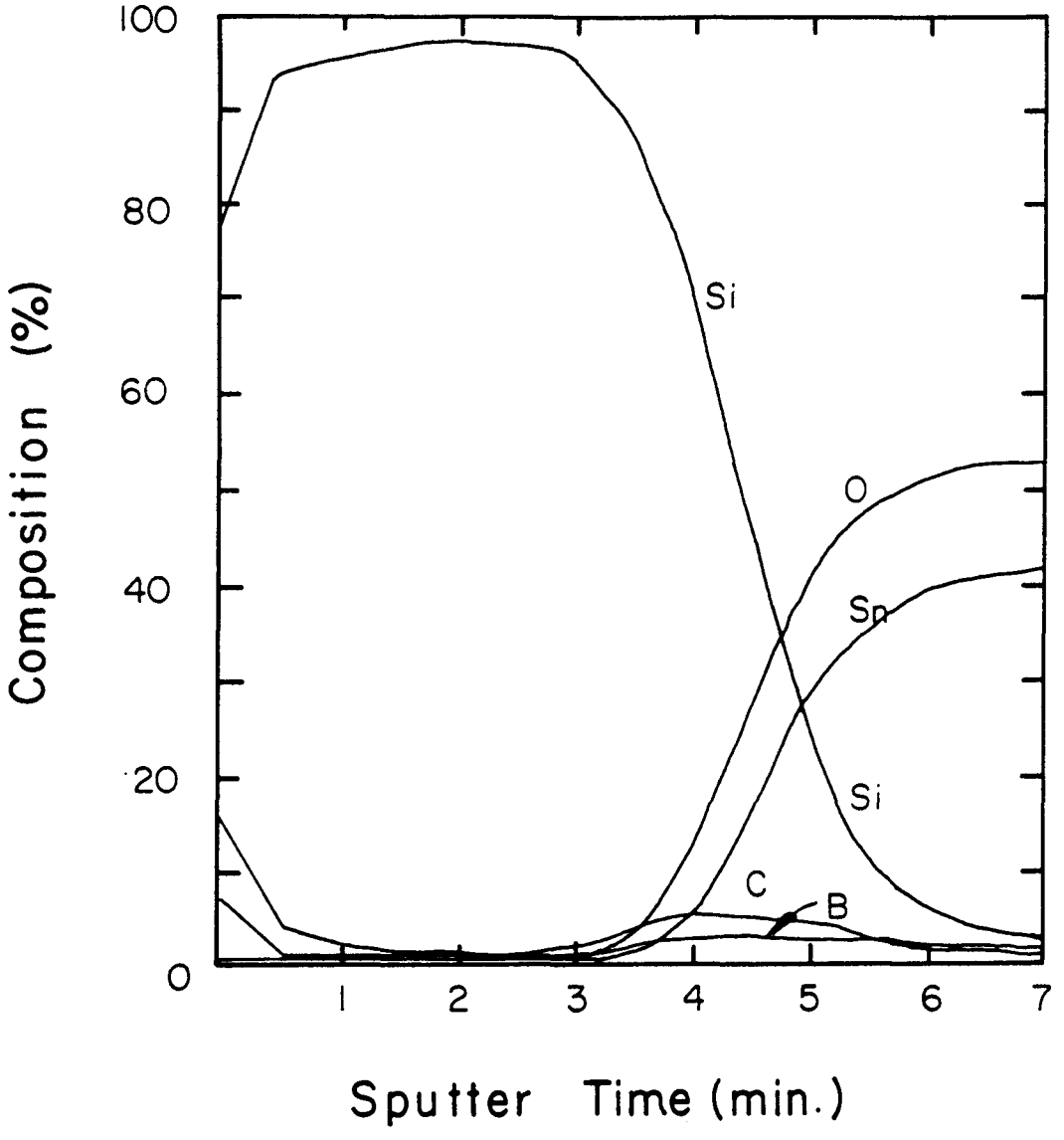

Fig. 16. Auger depth profile of ~400 A i a-Si:H/100 A p a-Si_xC_{1-x}/SnO_2/glass where amorphous silicon and silicon-carbide layers were prepared at 375 C. Tin is in the elemental state for sputtering time less than about 3.5 minutes.

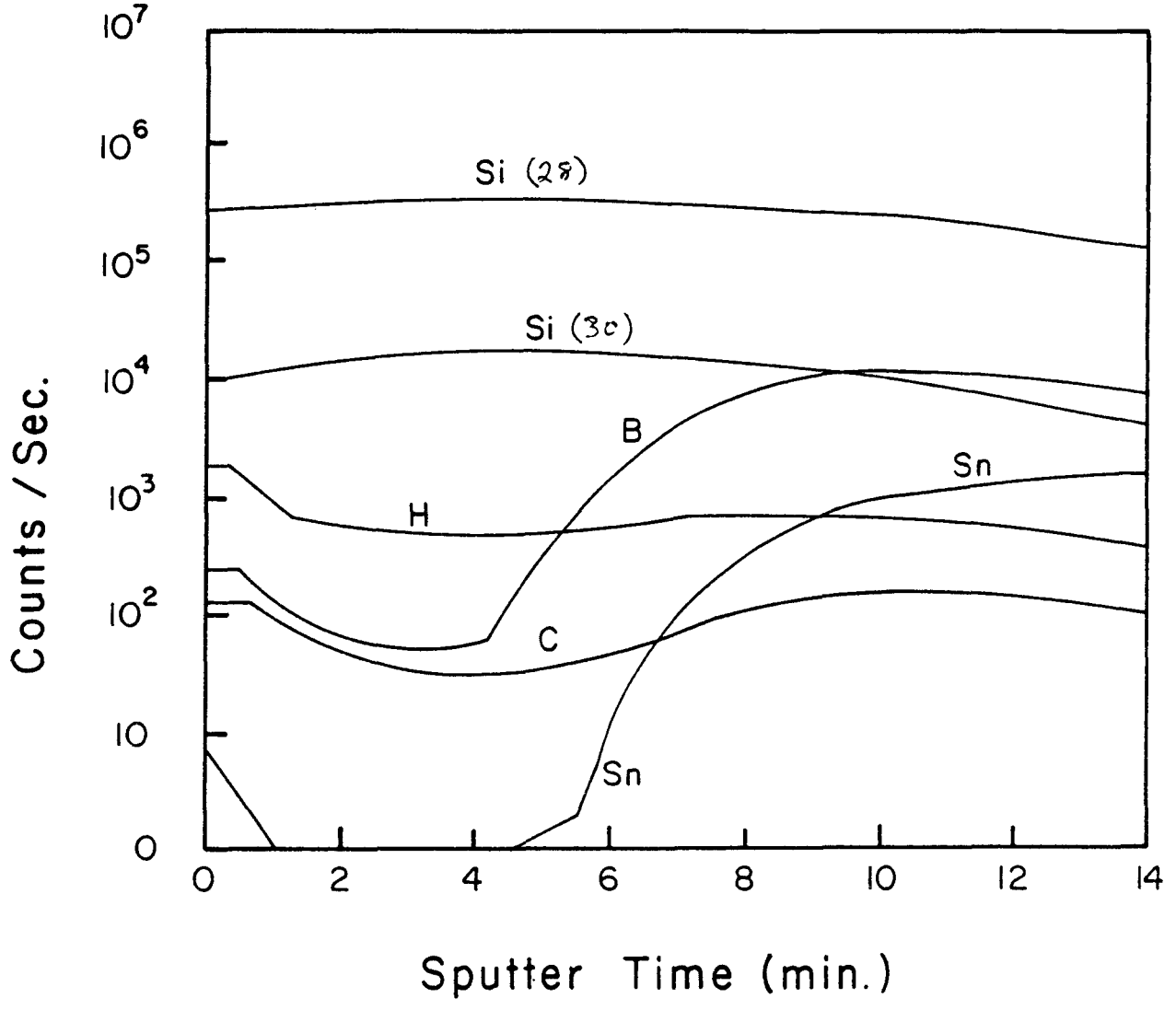

Fig. 17. SIMS depth profile of ~400 A i a-Si:H/100 A p a-Si_xC_{1-x}/SnO_2/glass where amorphous silicon and silicon-carbide layers were prepared at 375 C. The atomic hydrogen concentration after 3 minutes of sputterring is about 5.2%

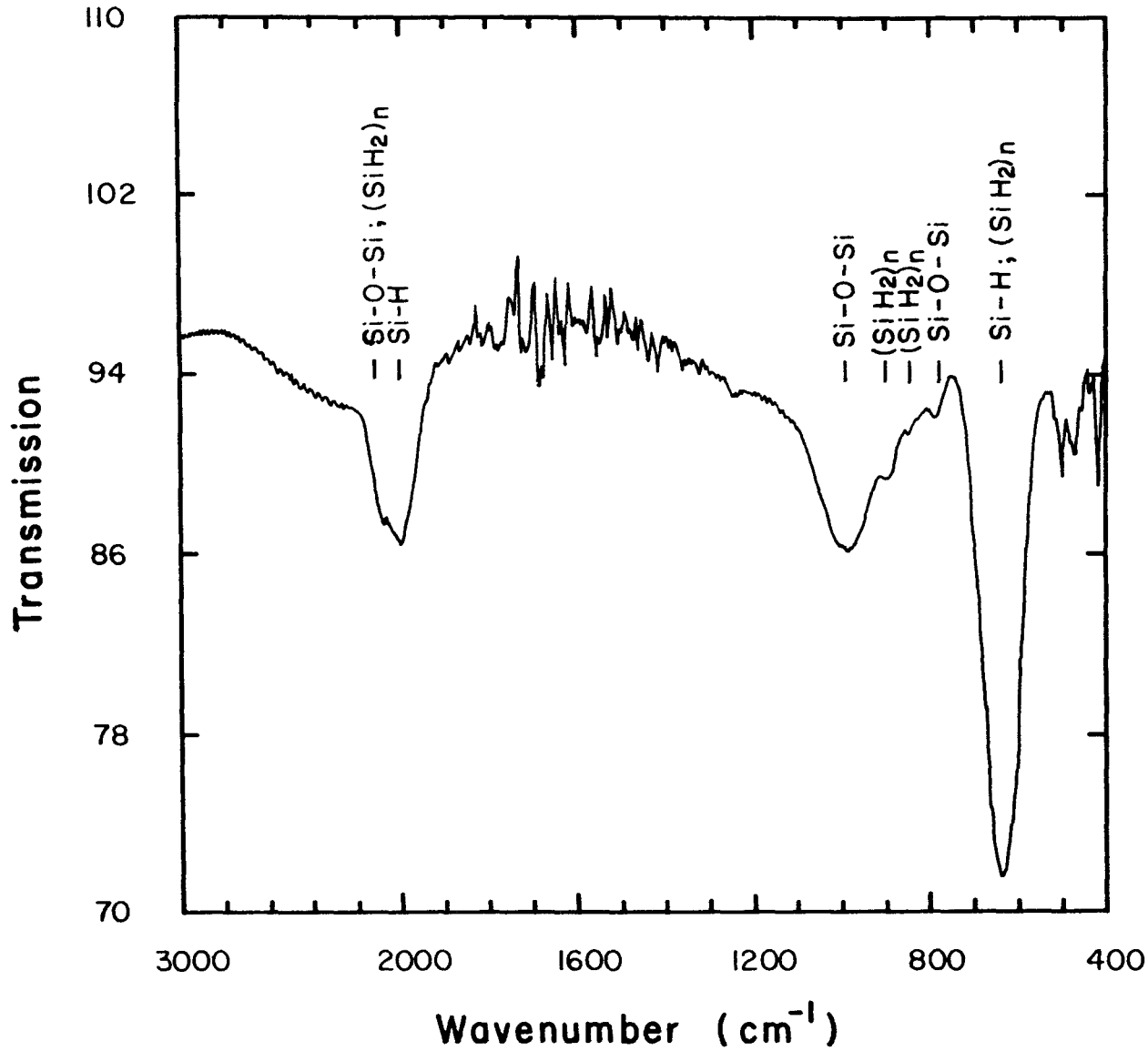

Fig. 18. Infrared transmission spectrum of an a-Si:H sample deposited at a high growth rate by photo-CVD.

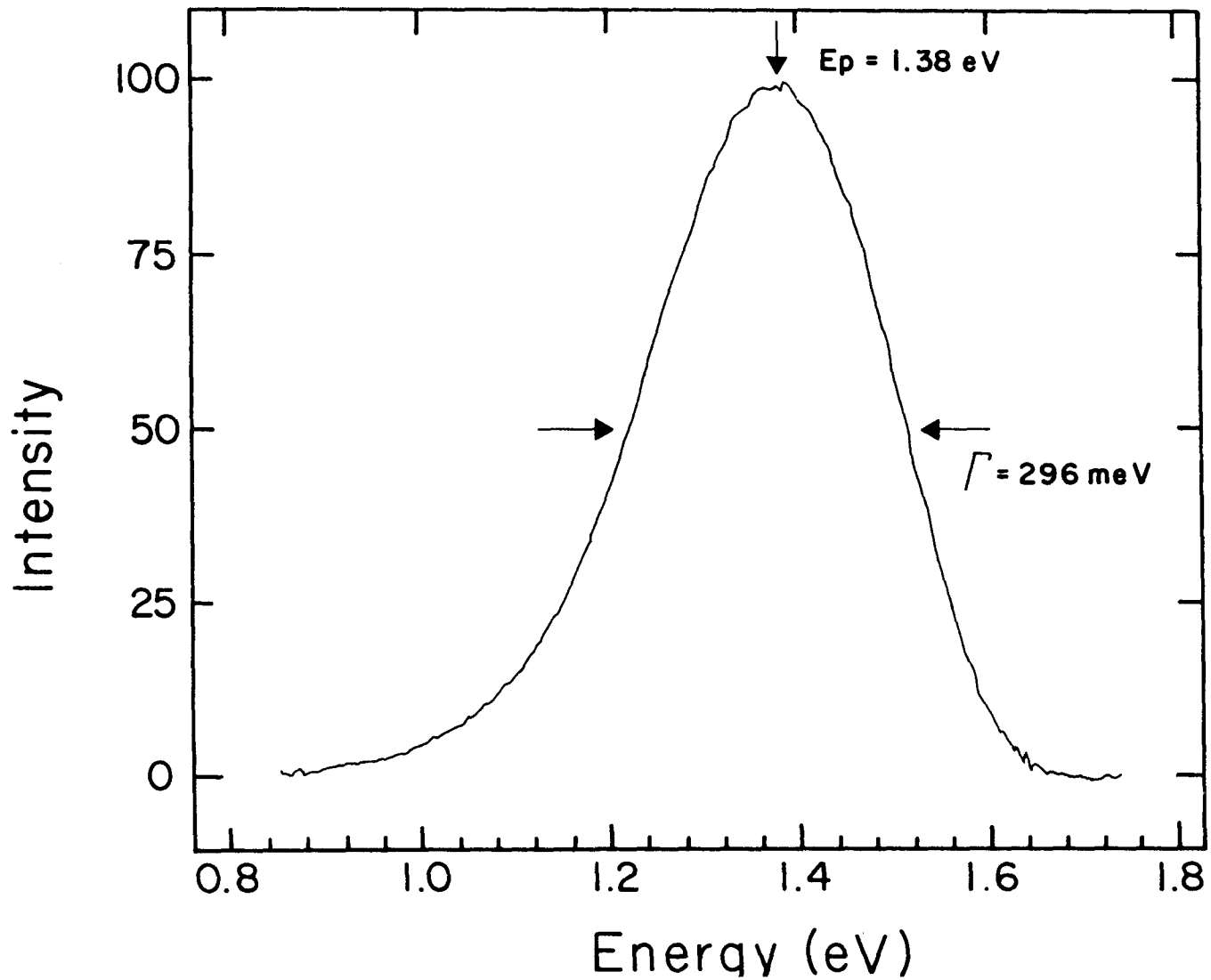

Fig. 19. Photoluminescence spectrum of an a-Si:H sample deposited at a high growth rate by photo-CVD.

SECTION 3
REFERENCES

1. T. Inoue, M. Konagai and K. Takahashi, Appl. Phys. Lett., 43, 774 (1983).

2. E.R. Austin and F.W. Lampe, J. Phys. Chem. 80, 2811 (1976).

3. T.L. Pollock, H.S. Sandhu, A. Jodhan and O.P. Strausz, J. Am. Chem. Soc. 95, 1017 (1973).

4. B. Reiman, A. Matten, R. Laupert and P. Potzinger, Ber. Bunsenges. Phys. Chem. 81, 500 (1977).

5. G.G.A. Perkins, E.R. Austin and F.W. Lampe, J. Am. Chem. Soc. 101, 1109 (1979).

6. P.E. Vanier, A.E. Delahoy and R.W. Griffith, J. Appl. Phys. 52, 5235 (1981).